Title

Carbohydrates at the Crossroads: A Multiscale View of the Role of Carbohydrates in the Face of Climate Change

Author

Orozco, Jessica

Publication Date

2023

Peer reviewed|Thesis/dissertation

Carbohydrates at the Crossroads: A Multiscale View of the Role of Carbohydrates in the Face of Climate Change

By

JESSICA OROZCO
DISSERTATION

Submitted in partial satisfaction of the requirements for the degree of

DOCTOR OF PHILOSOPHY

in

Horticulture and Agronomy

in the

OFFICE OF GRADUATE STUDIES

of the

UNIVERSITY OF CALIFORNIA

DAVIS

Approved:

Maciej A. Zwieniecki, Chair

Matthew E. Gilbert

Astrid Volder

Committee in Charge

2023

Dedication

To my family: Maria Del Refugio Renteria, Angel Orozco, Daisy Orozco and Angel Jr. Orozco whose unwavering love and support have shaped my journey and led to this milestone.
Love you!

Abstract

This research venture presents three distinctive studies, employing non-structural carbohydrate (NSC) measurements as an effective tool to evaluate plant responses under varied environmental conditions.

Chapter One focuses on how the rate of drought development impacts energy reserves and the recovery process in Grenache, a cultivar. The research studied fast-developing drought (FDD) and slow-developing drought (SDD). FDD, characterized by rapid stomatal closure and high abscisic acid (ABA) accumulation, showed negligible stem priming for recovery. However, SDD exhibited gradual stomatal closure, lower ABA accumulation, and changes preparing the stem for recovery, including xylem sap acidification and sugar accumulation. Both drought types showed similar trends concerning stomatal conductance recovery, yet displayed different sensitivities to xylem ABA. Total NSC content in plant stems was affected differently by FDD and SDD. FDD didn't significantly alter total carbohydrate content, whereas SDD led to an increase during stress, which normalized post-recovery. FDD resulted in a higher stem starch content during drought and post-rehydration, with no significant change in soluble sugar accumulation. SDD plants accumulated slightly more starch and significantly more soluble sugars, which returned to pre-stress levels swiftly after rehydration. This study indicates plants' unique adaptability to long-term drought and highlights the need for accurately reflecting field conditions when studying plant responses to drought.

Chapter Two investigates the impact of extended smoke exposure on NSC reserves in trees under natural field conditions. The study analyzed a comprehensive regional dataset and detailed spatiotemporal satellite data. Results showed that mid-growth season smoke exposure could transiently deplete plants' NSC reserves, while exposure later in the growth cycle could disrupt the vital carbohydrate reserve buildup, leading to a prolonged reduction in reserves. This introduces an unrecognized risk to plant health and ecosystem stability, threatening both agricultural and natural environments on a regional scale.

Chapter Three explores climate change implications on almond orchard phenology and the subsequent land suitability for almond farming. This study utilized historical climate data, a model incorporating daily minimum/maximum temperatures and NSC dynamics in twigs, and CMIP6 climate predictions. Analysis under two climate change scenarios projected that land suitable for almond farming could remain largely stable over the next three decades. However, under the unchanged emission scenario, the suitable land could see a reduction ranging from 50% to 95% by the century's end, aligning with a shift in bloom time. This signifies the critical role of climate change in shaping almond production's future, emphasizing the need for sustainable agricultural land management, ensuring long-term food security and economic stability amidst evolving climate conditions.

In conclusion, the research presents valuable insights into plants' adaptability and resilience under different environmental stressors. It demonstrates the importance of NSC measurements in understanding these responses, opening avenues for future research and effective adaptation strategies in the face of changing environmental conditions. It also underscores the pressing need

to address the risks and challenges posed by climate change and other anthropogenic factors to ensure sustainable agricultural practices and ecosystem stability.

Introduction

The future of our planet is critically dependent on understanding the complex interplay of natural systems in the face of escalating climate change. One crucial component of this intricate network is plants, who hold a pivotal role in the world's ecosystems and agriculture. As plants brace for an uncertain future characterized by intensified abiotic stressors such as drought, pollution, and temperature fluctuations, their resilience becomes increasingly important to study. This is particularly true for perennial species that bear the cumulative impact of recurring environmental challenges, as this could profoundly affect their productivity and survival.

A key component in plants' defense strategy against these stressors is their carbohydrate reserves. Serving as a plant's primary insurance policy, carbohydrates ensure immediate survival, future growth, and fecundity. These reserves, primarily composed of soluble sugars and starch, fuel current growth and metabolic activities. However, the role of carbohydrates transcends being just temporary energy reserves. They offer a reliable energy source for plants to utilize when external conditions are unfavorable or during prolonged periods of asynchronous carbohydrate supply, such as day-night cycles or seasonal changes. They also prove indispensable during longer-term environmental changes. For instance, under severe drought conditions, photosynthetic activity can halt, forcing plants to rely heavily on their carbohydrate reserves. Furthermore, they serve as a safety net, facilitating the restoration of vital functions following periods of stress, such as aiding the recovery of the plant's hydraulic system and ensure the regrowth of leaves or roots once stress conditions have subsided. Similarly, during the dormant winter months, these reserves are crucial for supporting essential functions and preparing the plant for the imminent growing season.

Given this pivotal role of carbohydrates, an understanding of their function and dynamics under various stress scenarios is fundamental to predict future plant dynamics and resilience. In this thesis, I will embark on a multiscale exploration of how carbohydrates help plants withstand a range of stressors, from drought and smoke exposure at the individual and regional level to the wider implications of climate change

on blooming patterns. My research presents a comprehensive view of the potential use of carbohydrate analysis for evaluating the stress response capacity of perennial plants. This investigation has been made possible through advancements in high-throughput carbohydrate analysis in woody tissue, notably the creation of a near-infrared (NIR) predictive model. This model enables spectral analysis of starch and sugar content in woody plants, offering a promising tool for understanding and assessing plant resilience to environmental stressors. This investigation will not only enhance our understanding of plant function under stress but also provide valuable insights into the future of plant dynamics in an era of changing climate. By unraveling these mechanisms, we can be better equipped to devise strategies that safeguard the resilience and productivity of our plant ecosystems and agricultural landscapes. My thesis is composed of three distinct yet interconnected chapters: (1) an exploration of plant-level responses to water stress, focusing on a single seasonal time scale; (2) a study of regional-level responses in the California Central Valley, assessing multi-year reactions to smoke pollution generated by wildfires; and (3) an examination of the impact of a warming climate on bloom shifts in almond trees. These chapters together aim to provide a comprehensive perspective on the interaction between plant physiology and various environmental stressors. (Citations included in Ch.1-3)

Ch. 1 Impact of drought progression rate on stress response and recovery in *Vitis vinifera*

Deciphering plant resilience against abiotic stressors like drought is limited, largely because research to date has primarily focused on elucidating the tactics plants utilize to resist stress and minimize irreversible harm and less so on the recovery process. In response to extreme drought, plants frequently suspend photosynthetic activity, shifting their reliance to carbohydrate reserves. In a scenario where reserves are already strained due to diminished photosynthesis, it's crucial for plants to strategize effectively to combat and recover from intensifying drought conditions. They face the considerable task of striking a balance between sustaining current metabolic processes and preserving sufficient resources for ensuring future functional recovery. This task becomes increasingly complex when considering the temporal

dynamics of stress, which include factors such as intensity, rate, and duration which can influence both the trajectory of drought progression and the ensuing plant recovery process.

The rate of drought progression can profoundly influence not only the total amount of nonstructural carbohydrates (NSCs), but also their distribution and composition. For instance, a rapid drought onset leading to reduced xylem sap pH could stimulate the accumulation of soluble sugars in the apoplast. These sugars, acting as osmolytes, generate a gradient crucial for refilling embolized conduits – a 'stem priming' process vital for recovery. Alternatively, a slower drought progression could require more gradual adjustments in carbohydrate metabolism and other physiological functions. Strategies like the gradual reestablishment of pre-stress functions might be necessary to afford adequate time for repairing drought-inflicted damage. This could involve delaying the reopening of stomata after tension alleviation, thereby limiting transpirational demand and allowing more time for the slow, osmotically driven removal of embolisms. Therefore, the race of drought development can considerably impact the path and extent of plant recovery. **In this chapter, our primary objective was to grasp how the rate of stress development affects energy reserves and influences the recovery process, underlining the need for further studies into how plants fine-tune their responses to varying drought progression scenarios.**

Ch.2 Assessing the Impacts of Prolonged Fires on Carbohydrate Reserves in Trees

An emerging, substantial, yet frequently overlooked hazard to crucial ecological processes is the escalating frequency of wildfires, especially prevalent in California. The wildfire season in this region typically aligns with the onset of fall, from May to September, a period that coincides with the peak accumulation of carbohydrates in trees. These fires not only wreak havoc directly through burns but also generate a significant amount of smoke that can linger in the atmosphere for weeks, if not months. This lingering smoke is loaded with harmful chemicals, including carbon monoxide and ozone. These pollutants can obstruct photosynthesis, curbing the tree's capacity to produce energy and accumulate carbohydrates. Moreover, the smoke modifies the intensity and quality of light reaching the trees, posing an additional

challenge to photosynthetic efficiency. **In this chapter, we present the repercussions of these alterations on the formation of carbohydrate reserves prior to dormancy in response to mid and late season fires in three major nut species (almond, walnut and pistachio) and the iconic California oak species (live oak).**

The decline in carbohydrate reserves could further disrupt flowering dynamics, influencing the timing and quality of bloom. This impact could cascade down to affect the tree's reproductive success and overall health. Our study leverages a unique opportunity to evaluate the effect of prolonged wildfire smoke on NSC reserves in four major tree species, both in natural and orchard environments. By integrating a long-term NSC dataset from the 'Carbohydrate Observatory' with the expansive and continuous monitoring provided by satellite aerosol detection (MODIS), we explore the consequences of sustained smoke exposure on trees' carbon reserves. Specifically, we analyze changes in NSC concentrations over time, comparing periods before and after smoke exposure. Our hypothesis is that prolonged exposure to high-intensity smoke depletes NSC reserves due to its inhibitory impact on photosynthetic activity.

Ch.3 Impacts of Historical and Projected Climate Change on Bloom Timing in California's Almond Orchards

Extreme events like droughts and wildfires are escalating at an unparalleled rate, reshaping the plant landscape dramatically. As sessile beings, plants find themselves in a precarious position and must adapt to these evolving conditions or face displacement by more adaptable species. For economically valuable crop plants, these changes pose a substantial threat to productivity. A failure to adapt could lead not only to a decrease in crop yield, but also potentially to a complete loss of certain crop varieties. The blooming period represents a particularly vulnerable time for plants, as the precise timing of this process plays a critical role in plant survival and reproduction. A particularly intriguing role of carbohydrates is their signaling function, crucial for perennials. These carbohydrate stores can act as signals that prompt plants to emerge from dormancy and initiate the process of blooming. This function is of utmost importance

in trees, where the timing of bloom significantly influences their survival and reproduction. An early bloom might expose them to the risks of late frosts, which can damage their delicate flowers, while a delayed bloom can miss peak pollinator activity, compromising their reproduction and productivity.

Furthermore, in the face of a rapidly changing environment, agricultural systems across the globe are grappling with escalating pressure. There's an urgent need to not only sustain but also enhance crop productivity, paradoxically, on a land base that is either shrinking or remaining constant. This dynamic is intensified by the burgeoning global population, which directly translates into increased demand for food, even as arable land is repurposed for urbanization or compromised by soil degradation. As we strive to boost productivity per unit of land, it's vital to recognize that the effects of climate change could potentially render certain lands unfit for production in the future. Alterations in temperature patterns, precipitation, and growing seasons, coupled with increased incidences of extreme weather events, could significantly impact the land's ability to support crops. Crops traditionally grown in specific regions might no longer thrive under changing climatic conditions, forcing agricultural systems to adapt either by transitioning to new crop varieties or completely altering their agronomic practices. In worst-case scenarios, productive lands could become entirely infertile, leading to decreased food production and posing a significant threat to food security. Therefore, as we look to the future, it's not merely about improving productivity within the current constraints but also understanding how we can adapt what we grow to changing conditions.

Here we employ a model integrating daily minimum and maximum temperatures, carbohydrate dynamics, and CMIP6 scenarios. Our objective is to delve into the future of the Central Valley's agricultural landscape, specifically focusing on how land suitable for productive bloom might transform in response to these evolving conditions. By employing this integrative approach, we seek to explore and predict how the Central Valley – California's agricultural heartland - might adapt and shift under different climate change trajectories outlined by the CMIP6 scenarios. We aim to provide insights into the resilience and adaptability of this region under future climatic uncertainties, highlighting the implications for agricultural productivity and sustainability.

Ch. 1 Do the ends justify the means? Impact of drought progression rate on stress response and recovery in *Vitis vinifera*

Morabito C[1]§, Orozco J[2]§, Tonel G[1], Cavalletto S[1], Meloni GR[3], Schubert A[1], Gullino ML[3], Zwieniecki MA[2*], Secchi F[1*]

[1]) Department of Agriculture, Forest and Food Sciences, University of Turin, Largo Paolo Braccini 2, 10095 Grugliasco (Italy)

[2]) Department of Plant Sciences, University of California Davis, One Shields Avenue, 95616 Davis (CA), USA

[3]) Agroinnova - Centre of competence for innovation in the agro-environmental field, Largo Paolo Braccini 2, 10095 Grugliasco (Italy)

§-* equal contribution authors

Published in *Physiologia Plantarum* on 22 October 2021

Abstract

Plants are frequently exposed to prolonged and intense drought events. To survive, species must implement strategies to overcome progressive drought while maintaining sufficient resources to sustain the recovery of function. Our objective was to understand how stress rate development modulates energy reserves and affects the recovery process.

Grenache *Vitis vinifera* cultivar was exposed to either fast developing drought (within few days; FDD), typical of pot experiments, or slow developing drought (few weeks, SDD), more typical for natural conditions.

FDD was characterized by fast (2-3 days) stomatal closure in response to increased stress level, high ABA accumulation in xylem sap (>400 μg/L) without the substantial changes associated with stem priming for recovery (no accumulation of sugar or drop in xylem sap pH). In contrast, SDD was characterized by

gradual stomatal closure, low ABA accumulation (<100 μg/L) and changes that primed the stem for recovery (xylem sap acidification from 6 to 5.5 pH and sugar accumulation from 1 to 3 g/L). Despite FDD and SDD demonstrating similar trends over time in the recovery of stomatal conductance, they differed in sensitivities to xylem ABA. Grenache showed near-isohydric and near-anisohydric behavior depending on the rate of drought progression gauging the risk between hydraulic integrity and photosynthetic gain. Isohydry observed during FDD could potentially provide protection from large sudden swings in tension whilst switching to anisohydry during SDD could prioritize the maintenance of photosynthetic activity over hydraulic security that is not threatened by a gradual increase in tension.

Key words: water stress rate, recovery, Abscisic acid, carbohydrates

Introduction

Over the course of their life, plants experience a wide range of climatic conditions, fluctuations in temperature, nutrient and water availability that are often suboptimal and can severely constrain their growth and reproductive development (Zeppel et al. 2014, Yuan et al. 2019). Perennial species in particular are left increasingly vulnerable to additional abiotic and biotic stressors, greatly limiting productivity (Allen et al. 2010). Amongst abiotic stressors drought is the most pervasive; plants recurrently face alternating periods of drought, varying in length and intensity, followed by the sudden availability of water often in the form of rain. Typically, under natural conditions, slow-developing drought spans weeks if not months (Zargar et al. 2011). Initially, the onset of drought leads to a drop-in plant water potential and stomatal conductance consequently hindering photosynthesis and impeding growth. Prolonged exposure to stress results in xylem embolism formation thus interrupting and/or completely halting water transport, which if not ameliorated may culminate in plant death (Tyree and Sperry 1989, Zwieniecki and Secchi 2015). Plant stress response strategies emerged to account for drought severity, duration, and frequency typical of their respective environments, with the goal of utilizing the sudden burst of water supply to resume physiological activity. Therefore, species survival strategies to cope with drought stress cannot just be seen as passive,

but rather as proactive preparations for recovery prompted by the sudden availability of water. This novel premise stipulates that drought and recovery are not dichotomous and independent but should be considered as one interwoven continuous process (Ruehr et al. 2019).

Processes that lay the foundation for facilitating recovery may be activated alongside conventional stress response mechanisms. Given that preparation for recovery is initiated during drought, its course and effectiveness may be impacted by features characteristic of temporal stress dynamics such as rate, and duration, which may dictate the ultimate success of post-drought recovery (Anderegg et al. 2013). Much of our current understanding rests upon studies performed on plants, more than often maintained in pots and greenhouses, wherein drought is simulated by an abrupt discontinuity in water supply, which can skew or even completely overlook the processes at play during the natural trajectory of drought stress (Romero et al. 2017). In nature, stress usually develops gradually over the course of weeks or months as effective soil volume per plant is large, while in experimental settings large negative tensions are often achieved in a matter of a few days or even hours, thus altering or inhibiting acclimation responses and limiting our ability to reliably assess recovery dynamics (Ingrisch and Bahn 2018). In order to survive, species must be able to coordinate an arsenal of multiscale responses, including adjustments to their biochemistry and physiology that can concurrently address the progressive drought while maintaining sufficient resources to sustain the prospective recovery of plant function. These adjustments include changes in levels of stress hormones (Daszkowska-Golec and Szarejko 2013), osmolytes and protective chemicals (Blum 2017), xylem sap pH (Secchi and Zwieniecki 2012), metabolism of nonstructural carbohydrates (NSC) (Trifilo et al. 2017, Tomasella et al. 2019), and expression of genes (Cramer et al. 2007). Therefore, the length and severity of stress incurred by plants can have downstream ramifications on the degree and path of recovery. How and which aspects of stem biochemistry and whole plant physiology are affected by the rate of drought stress progression and how these changes impact recovery remains an open question.

Mounting evidence points to the linkage between NSC metabolism and a plant's capacity to cope and recover from drought stress (O'Brien et al. 2014, Schwalm et al. 2017, Trugman et al. 2018, Pratt et al. 2021). Amidst periods of water scarcity, during which stomatal closure prevents photosynthetic carbon

uptake (McDowell et al. 2008, McDowell et al. 2011), stored NSC can act as a buffer providing carbon to maintain basic metabolism and defense processes (McDowell and Sevanto 2010, Sala et al. 2012). Drought affects not only the total carbohydrates amount, but also the allocation and composition of NSCs, all of which can be linked to concurrent changes in xylem sap chemistry (Savi et al. 2016, Tomasella et al. 2017, Ivanov et al. 2019). Specifically, in some species, a drop in xylem sap pH induces an accumulation of soluble sugars in the apoplast that can promote recovery by serving as osmolytes generating a gradient to refill embolized conduits; processes that are associated with 'stem priming' for recovery (Secchi and Zwieniecki 2012, Pagliarani et al. 2019, Tomasella et al. 2021). Given that sugar depletion is expected during prolonged drought stress, rapid recovery of plant photosynthetic capacity might be a crucial adaptation that would confer plants with a competitive advantage. However, a gradual reinstatement of pre-stress functions may be necessary to afford sufficient time to repair drought stress related damage. For example, delaying stomatal opening despite tension alleviation may reduce transpirational demand and provide additional time for the slow osmotically driven removal of embolism to occur. In this respect, ABA-mediated control of stomatal aperture may be more important over passive turgor and water potential-driven responses. Thus, the objective of this study was to understand how plants use their time under stress to modulate their energy reserves (mostly carbohydrate supply) and xylem chemistry (pH and ABA content) to enhance recovery processes.

As sessile organisms subjected to a wide range of constantly changing environmental conditions, plants' survival depends on their capacity to integrate information about their surroundings, gauge potential trade-offs and adjust their physiology accordingly, all the while optimizing resources especially under water stress. Therefore, mechanisms that regulate gas exchange and restrict water loss are imperative for adapting and thriving in these conditions. While duration and magnitude are defining features of drought, the rate of stress progression is seldom considered despite its potential importance for the acclimation of plants to stress and their subsequent recovery. Therefore, we hypothesized that a slow developing drought (SDD) would permit the time for changes in the xylem sap chemistry to prime the stem for recovery while delaying stomatal opening. A fast-developing drought (FDD) would be limited to prioritizing the conservation of

water by shutting stomata without the changes associated with stem priming. Given that stomatal behavior can have large implications for NSC and water-loss dynamics, we tested our hypothesis on *Vitis vinifera* cultivar Grenache purported to be near-isohydric (Shelden et al. 2017). We evaluated stress responses and recovery by analyzing both physiological and chemical parameters in response to fast and natural timing of drought occurrence, thus investigating the specific drought response strategies.

Materials and methods

Plant materials and experimental set up

Vitis vinifera cv Grenache cuttings were provided by the nursery Vivai Cooperativi Rauscedo-San Giorgio della Richinvelda (PN), Italy. These commercially available plants are typically grafted on rootstock 1130P (V. berlandieri cv. Resseguier nr. 2 × V. rupestris cv. Du Lot.). In this study, we refer to the plants simply as Grenache.

Two-year-old grapevines were grown in a greenhouse under partially controlled climatic conditions. Temperature and relative humidity were maintained along the experiment in the range of 22–31°C and 40-80%, respectively (daily average temperature and relative humidity are reported in Table S1). Natural daylight was supplemented, when necessary, with light from metal halogen lamps to maintain a minimum of 500–600 mmol photons m^{-2} s^{-1} during a 12-h-light/12-h-dark cycle. Each plant grew in a 4-L pot filled with a substrate composed of sandy-loam soil/expanded clay/peat mixture (2:1:1 by weight). A total of 25 grafted grapevines with 1-5 branches per plant were used in this study. At the beginning of the experiment Grenache plants had an average length of 87.05 ± 11.8 cm (as measured from the graft union) and were characterized by the same phenological phase, with at least 10 fully expanded leaves at the scion thus assuring its photosynthetic independence. Furthermore, the plants remained in a vegetative phenological state through the extent of the experiment.

The 25 grapevines were further divided in 3 groups: 10 plants were exposed to SDD treatment, 10 plants to a FDD and the remaining 5 grapevines were kept as controls (CTR), these plants were irrigated to field capacity every morning during the whole experimental period. The SDD was achieved by progressively

reducing the amount of water provided to the plants along the experiment (20% less of water used every day), while the FDD was induced by interrupting irrigation (Fig. S1). The daily water loss for both FDD and SDD is shown in Fig. S2. In both treatments, water stress was imposed until stem water potential reached an average level of -2 MPa. Once water stress levels were reached, the grapevines were re-watered in the morning up to field capacity and for the following ten days (REC).

Xylem sap and stem tissues were collected from the treated (SDD, FDD and REC) and control plants (CTR) throughout the experiment duration and the samples were stored for further chemical analyses. Physiological parameters (stem water potential, stomatal conductance and photosynthesis) were monitored during the entire experiment (i.e. from the start of the stress treatments until full recovery of physiological functions) in both droughted and control plants. Since sampling for the biochemical properties of xylem sap was destructive, we randomly removed at least three lateral branches per treatment (one branch per plant) on every sampling date. Sample pooling was every 6 days for FDD, encompassing three periods (FD1–FD3), and every 12 days for SDD, encompassing four periods (SD1-SD4). During recovery, stem water potential recovered within one day for both treatments so pooling was done for day one (FR1, SR1) and then for the remaining recovery period (FR2, SR2).

Measurement of leaf gas exchange and xylem pressure

Stomatal conductance (g_s) and net photosynthesis (A_n) were measured on fully expanded leaves exposed to direct sunlight, using a portable infrared gas analyzer (ADC-LCPro+ system, The Analytical Development Company Ltd, Hoddesdon, UK). Measurements were performed using a 6.25 cm^2 leaf chamber equipped with artificial irradiation (1200 µmol photon m^{-2} s^{-1}), set with a chamber temperature of 25°C to avoid overheating. CO_2 values were maintained at greenhouse conditions (400-450 ppm). Leaf gas exchange was monitored daily (between 10:00 am and 12:00 pm) on three to five plants in each treatment (one leaf per plant) for the whole duration of the experimental trial. Meanwhile every 2-3 days three leaves per treatment (each from different plants) were collected for xylem pressure measurements (stem water potential).

Xylem pressure measurements were performed on fully expanded non-transpiring leaves. Prior to taking the measurements, leaves were placed in humidified aluminum foil-wrapped plastic bags for 20 minutes before excision. After excision, leaves were allowed to equilibrate for an additional 15 minutes and water potential was measured using a Scholander-type pressure chamber (Soil Moisture Equipment Corp., Santa Barbara, CA, USA).

Sap and stem sampling procedure

Xylem sap was collected from treated (SDD, FDD and REC) and control (CTR) plants, according to a previously described method (Secchi and Zwieniecki 2012). Briefly, a branch was attached through a plastic tube to a syringe needle. The needle was threaded through a rubber cork to a vacuum chamber, with the needle tip placed in a 1.5-mL plastic tube. After a vacuum suction was generated, pieces of stem were consecutively cut from the top, allowing liquid from open vessels to be sucked out of the stem and collected in the tube. Sap samples were stored at -20°C until analyses of pH and NSC content were conducted.

The stems sampled for sap collection were cut in small sections using a fresh razor blade and microwaved at 700 W for 3 min to stop enzymatic activities. Samples were then oven-dried at 70 °C for 24 h, ground to fine powder (particle size < 0.15 mm) using a tissue lyser system (TissueLyser II, Qiagen), and kept for further analyses (starch and soluble sugar content) at room temperature.

Measurements of pH and soluble carbohydrates in xylem sap

Variations in xylem sap pH during SDD and FDD and along recovery period in comparison to control plants were evaluated using a micro pH electrode (PerpHect® ROSS®, Thermo Fischer Scientific, Waltham, MA USA). Non-structural carbohydrates (NSC) content in xylem sap samples was quantified following the anthrone-sulfuric acid assay described by Leyva et al. (2008) with the modifications indicated in Secchi and Zwieniecki (2012). In short, 50 µL samples were mixed with 150 µL of anthrone in sulfuric acid (0.1%, w/v) in a 96-well micro-plate (iMark Microplate Absorbance Reader, BioRad). The plate was cooled on ice for 10 minutes, heated at 100 °C for 10 minutes, and then equilibrated to room temperature

for 10 minutes. A glucose standard curve was used to compare the colorimetric response of the samples, whose absorbance was read at 620 nm. Soluble carbohydrates concentration was expressed as g L^{-1} of glucose.

Analysis of soluble sugars and starch concentration in stem samples

25 ± 4 mg of powdered sample materials were transferred into a 1.5 mL Eppendorf test tube. To extract soluble sugars, 1 mL of 0.2 M sodium acetate buffer solution (pH= 5.5) was added to each sample, vortexed and incubated at 70°C for 10 minutes. The NSC were quantified following the procedure described above and the sugar concentration was expressed as mg g^{-1} dry weight. For starch analyses, the remaining pellet was exposed to 100°C for 10 minutes and submitted to enzymatic digestion for 4 h at 37°C in 0.2 M sodium acetate buffer (pH = 5.5) with 0.7 U of amylase and 7 U of amyloglucosidase. Once the digestion was completed, samples were centrifuged for 5 minutes at 21000 *g*, and the supernatant was diluted 1:20 and quantified using the method described above for determining soluble carbohydrates content.

HPLC-MS/MS analysis of sap abscisic acid (ABA) content

ABA concentration was quantified following the method described by Siciliano et al. (2015) with minor changes. Xylem sap samples were centrifuged at 13000 *g* and 4°C for 5 minutes. From the obtained supernatant, a total volume of 50 µL for each sample was collected in a 1 mL amber glass vial containing an appropriate glass insert (Supelco, Sigma-Aldrich) for small sample volumes and analyzed by HPLC-MS/MS. High Performance Liquid Chromatography was carried out using a 1260 Agilent Technologies (Waldbronn, Germany) system equipped with a binary pump and a vacuum degasser. Sample aliquots (20 µL) were injected on a Luna C18 (150 × 2 mm i.d., 3 µm Phenomenex, Torrance, CA) and ABA was eluted in isocratic conditions of 65:35 (H2O:CH3CN v/v acidified with HCOOH 0.1%) under a flow of 200 µL min^{-1} for 5 minutes. Using an electrospray (ESI) ion source operating in negative ion mode, samples were introduced into a triple-quadruple mass spectrometer (Varian 310-MS TQ Mass Spectrometer). Analyses were conducted in MRM mode using two transitions: 263>153 (CE 12V) for quantification, 263>219 (CE

12V) for monitoring, with 2 mbar of Argon (Ar) as collision gas. The external standard method was applied to quantify ABA concentration in target samples. In detail, a standard curve was generated using an original ABA standard (Sigma Aldrich, St Louis, MO, USA; purity 98.5%), with concentrations ranging from 10 to 500 µg L^{-1}. The detection (LOD) and quantification (LOQ) limits were calculated based on the standard deviation of the response (σ) and slope of the calibration curve (S) ratio in accordance with the ICH Harmonized Tripartite Guideline expressed as: LOD=3.3σ/S; LOQ=10σ/S. Calculated final values were as follows: LOD = 0.87 ng mL^{-1}; LOQ = 2.90 ng mL^{-1}.

Statistical analyses

Significant differences among treatments were analyzed by applying a one-way analysis of variance. Fisher LSD significant difference post-hoc test was used for separating means when analysis of variance results was significant ($P < 0.05$). The SPSS statistical software package (v24.0, SPSS Inc., Cary, NC) was used to run the statistical analyses, and Sigma Plot software (Systat Software Inc., San Jose, CA) was used to create figures.

Results

Physiological Changes in Response to SDD, FDD and Recovery

Using two distinct methods to impose drought onto potted plants: (1) an immediate interruption of irrigation resulting in fast developing drought (FDD) and (2) a constant reduction in available water resulting in slow-developing drought (SDD), we successfully implemented two rates of drought progression allowing us to test the proposed hypotheses. Grenache plants exposed to SDD reached the stress level of approximately -2 MPa in 44 days (ψ stem: -2.06 ± 0.40 MPa), while in FDD water stress was achieved within 18 days (ψ stem: -1.85 ± 0.07 MPa; Fig. 1a). The rate of water stress progression was significantly different between treatments and was ~0.09 and ~0.025 (MPa day^{-1}) respectively for FDD and SDD (Fig. 1a). Stomatal conductance (g_s) progressively decreased during SDD treatment, while it seemed to collapse within 1 day in FDD treatment (Fig. 1c). The response of g_s to xylem pressure was different between the two treatments;

in the SDD treatment plants gradually shut stomata in response to increment of stress level and remain partially open even at -1 MPa, while in FDD stomata closure occurred at the onset of low stress around -0.6 MPa (Fig. 2a). Post-rewatering, water potential recovered within the first day in both treatments (Fig. 1b). Recovery of g_s was much slower than that of water potential but was not significantly affected by treatment (Fig. 1d). Recovery of g_s expressed as a response to water potential revealed no relationship (Fig. 2b).

As expected, net photosynthesis and stomatal conductance were well correlated; a constant reduction of net photosynthesis was in fact coupled with a progressive reduction of g_s (Fig. S3a). Rewatering completely restored photosynthetic activity to pre-stress measurements after stomata were fully open (Fig. S3b).

At the end of the treatments, well irrigated plants were longer than the stressed ones (165.67 ± 15.04 cm versus 107 ± 5.3 cm and 132.25 ± 11.32 cm, respectively for SDD and FDD treatments). The plants exposed to SDD at the end of experiment showed a 23% of stem length increment, while Grenache exposed to FDD were about 52% longer than plants at the beginning of experiment (Fig. 3). Moreover, SDD grapevines grew only the first 13 days from the beginning of the stress.

Biochemical Changes in xylem sap in Response to Stresses and Recovery

Xylem sap ABA increased with the increment of drought level for both stresses (Figs. 4b and S4b), however ABA was highly accumulated at the end of FDD treatment (FD3, Fig. 4b). The ABA accumulation to 60-90 □g/L forced complete stomatal closure (Fig. 1c), but ABA continued accumulation under FDD treatment and reached values 10 times higher than those under SDD conditions. During the recovery phase, xylem pressure recovered within one day, however ABA concentrations during the few hours and 1 day post recovery (R1, Fig. 4b) remained high at the level of FDD and SDD under drought. Drop in ABA content did not occur until 8-10 days post rehydration. At that time, ABA concentration decreased to pre-stress values in both treatments (R2, Figs. 4b and S4b).

During FDD and SDD, the response of ABA to stomatal conductance was well correlated in both drought treatments; FDD: $R^2 = 0.98$ $P < 0.001$, SDD: $R^2 = 0.92$ $P < 0.001$ (Fig. 5). The ABA concentration increased

significantly in the xylem sap of the stems while g_s decreased and a maximum level of ABA was reached when stomata were closed.

Fast developing drought did not significantly affect the pH of xylem sap. Sap acidification was observed after one day of relief from slow developing drought (Fig. S4). Xylem sap pH changed from of 5.92 ± 0.042 in control plants to 5.46 ± 0.12 in recovered plants (Fig. 4c). The acidification of xylem sap occurred in parallel with a significant increase in soluble carbohydrate content (from 0.51 ± 0.079 g L^{-1} in control plants to 3.82 ± 1.16 g L^{-1} in recovered plants; Fig. 4d). The total amount of carbohydrates in the sap returned to pre-stress levels after 10 days of rehydration (0.44 ± 0.056 g L^{-1}), when pH values were higher and overlapping those of irrigated plants (pH: 5.75 ± 0.053; Fig. 4d). During the drought experiments, sugar concentration was low and not correlated with pH values (Fig. 6). However, Grenache SDD stressed plants showed high carbohydrate content only at lower pH values during the first day of recovery (SR1) that was significantly different from the rest of the measurements (Fig. 6).

Biochemical Changes in stem tissues in Response to Stresses and Recovery

Drought treatments affected differently the total NSC contents in the stems; plants exposed to FDD treatment did not modify the total carbohydrates (starch plus soluble sugars) content in stem tissues during both stress and recovery (Figs. 7a and S5). However, plants exposed to SDD showed an increase of total NCS content during stress and the values returned to pre-stress levels when water was alleviated, with sugar concentration overlapping those of well-watered grapevines, (SDD: 94.32 ± 26.40, 157.97 ± 19.55 and 105.23 ± 2.75 mg g^{-1} of total sugars respectively for well-watered, SD4 stress and recovered plants; Fig. 7a).

In details, the FDD treatment increased the content of starch in the stems during the drought imposition (FD3, 1.5-fold more than controls) and after one day of rewatering (2.2-fold more, Fig. 7b), while the accumulation of soluble sugars did not change over the experiment (Fig. 7c). Plants from SDD treatment accumulated slightly more starch compared to well-watered conditions (Fig. 7b) and significantly more

soluble sugars (1.7-fold more). Interestingly, during the recovery phase stem sugars in SDD plant return to pre-stress level within one day (Fig. 7c).

Discussion

The two methods adopted to impose drought on potted grapevines were chosen to simulate the fast water potential decline, rates of ~0.09 (MPa day^{-1}), typical of most drought experiments conducted on potted plants (Griesser et al. 2015) and the gradual decline, rates of ~0.025 (MPa day^{-1}), more typical of drought under field and natural conditions (Romero et al. 2017). We found significant differences between the fast and slow rates of drought progression, among the measured water stress related physiological responses including stomatal conductance, xylem sap ABA concentration, xylem sap pH, and soluble sugar concentrations in xylem sap, as well as modifications in the content of stem carbohydrates. Furthermore, we observed that not only was each drought rate accompanied by distinct xylem biochemical changes but in addition, the respective changes also set the precedent for their corresponding recovery. However, we also observed similarities between the two treatments particularly in the trajectory of water potential and g_s during the recovery. Taken together, our findings suggest that the evaluation of plant response to stress should be analyzed in the context of plant water potential, while the subsequent response to recovery from stress should be evaluated in the context of time, as xylem pressure immediately returned to pre-stress levels in both treatments. Moreover, our findings can be analyzed in the context of the impact of drought progression rate on protective strategy (isohydric vs anisohydric behavior) and the subsequent recovery process.

A binomial method of classification, isohydric and anisohydric (Schultz 2003), has been used to explain differences in stomatal behavior between *Vitis vinifera* varieties in response to water stress. However, this classification should not be decisive (Hochberg et al. 2018), and recently it has been shown that isohydric and anisohydric behavior is not constitutive for a characteristic variety but rather it is environmentally dependent (Martorell et al. 2015). In general, anisohydric plants, withstand a wide variation of water potential but promote photosynthetic gains, thus maintaining higher stomatal aperture

and exhibiting substantial reduction in xylem pressure (Coupel-Ledru et al. 2017). In contrast, isohydric plants should limit water potential variation to protect hydraulic integrity at the cost of photosynthetic output and are more exposed to carbon starvation risk when compared to anisohydric plants, due to the prompt stomatal closure in the case of water stress (Tardieu and Simonneau 1998). Grenache is typically considered to show near-isohydric response. Indeed, when exposed to FDD, Grenache shut stomata in a step-like manner in response to small drops in water potential (within 0 to -0.6 MPa) in a manner to the typical isohydric stomatal behaviors. However, Grenache's isohydric behavior disappeared under the SDD treatment. Such dual response contradicts popular approaches that ascribe species or varieties' dominant adaptive stomatal responses to be inherent and independent of environmental conditions (Dal Santo et al. 2016).

Some previous studies have reported switching between iso- and anisohydric behavior even within the same cultivar (Franks et al. 2007, Chaves et al. 2010, Rogiers et al. 2012, Zhang et al. 2012), but the circumstances promoting this behavioral ambiguity in response to drought remained unclear (Domec and Johnson 2012, Klein 2014). Considering stress development dynamics may reconcile the apparent inconsistencies and provide insight into the benefits that come from a shifting strategy that adjusts along a stress continuum as opposed to being constrained to an archetypal response. Isohydricity may be a beneficial response under FDD regimes when sudden unanticipated deviations from typical transpirational demand risk exposure to tensions that can endanger xylem functionality (Tyree and Sperry 1988) or accelerate senescence. Under SDD conditions a near-anisohydric response can dominate, as a slow buildup of tension affords plants the time and security to better acclimate under the reduced risk of sudden hydraulic failure, all the while preserving photosynthetic activity. In this study, Grenache exemplifies such flexibility by modulating stomatal conductance in accordance with drought length and rate. Thus, we suggest that iso- and anisohydric behaviors bound an array of facultative behaviors imposed by different rates and length of drought stress that permit plants to shift priorities and coordinate responses to optimize the tradeoff between carbon gain and hydraulic function, and analysis of stomatal response to water stress should account for the rate of stress development.

Xylem sap ABA and pH have been shown to mediate stomatal closure and linked to aniso- and isohydric behavior (Davies et al. 2002, Sharp and Davies 2009, Marusig and Tombesi 2020). In fact, both strategies are often associated with different degrees of ABA concentration and sensitivity (Coupel-Ledru et al. 2017). Under FDD, following a moderate decrease in water potential, a steep decline in stomatal conductance was observed along with a large and sudden increase of ABA concentration in xylem sap. Maximum ABA levels were achieved following complete stomatal closure, which may explain the high post stomatal-closure foliar ABA accumulations observed in previous studies (Tombesi et al. 2015, Frioni et al. 2020). Under SDD, the increase of ABA concentration was very slow and reached levels 10 times lower than those under the FDD treatment. While the maximum level of ABA stood in stark contrast between the two treatments, in both cases ABA progressively increased at the onset of drought concurrent to the decline in g_s with complete stomatal closure occurring under similar ABA concentrations (60-80 □g/L). The high accumulation of xylem ABA observed under FDD conditions but not under SDD conditions is a surprising observation suggesting that ABA production by roots in response to stress may be related not to stress severity but to rate of its occurrence. In addition, the excessive increase in ABA concentration observed in the FDD treatment might suggest lower sensitivity of stomata to ABA concentration under sudden drought (see slight shift in response of g_s to ABA in Fig. 5 inset). This might indicate that ABA sensitivity is not an intrinsic varietal property but can be associated with the rate of water stress development. Therefore, ABA sensitivity may not be the best indicator to differentiate between iso/anisohydricity given that stress rate progression might alter ABA sensitivity and patterns of accumulation. We think that this notion is a novel concept that should be further explored as previous studies have found that experimental conditions influence stomatal behavior and apparent sensitivity to ABA (Lavoie-Lamoureux et al. 2017, Martinez-Vilalta and Garcia-Forner 2017).

Moreover, the ABA concentration in the xylem sap and plant sensitivity acquired during stress may also play an important part in recovery from stress. There is an increasing appreciation for the fact that the recovery of water potential does not result in immediate stomatal opening (Blackman et al. 2009, Martorell et al. 2014) and delay is often observed. Such time-lag may be an evolved trait that provides additional time

for the restoration of hydraulic plant capacity (Martorell et al. 2014, Pagliarani et al. 2019). This delay has been associated with lingering ABA concentrations post-tension-release (Lovisolo et al. 2008, Brodribb and McAdam 2013). Indeed, in the present study we observed the presence of lingering ABA following rehydration. One might expect that gas exchange recovery from fast induced stress would be hastened by the quick improvement in water potential. Surprisingly, the recovery of leaf gas exchange was slow and not related to the recovery of water potential in both drying regimes despite levels of lingering ABA being drastically lower in SDD than in FDD. It can be speculated that recovery in Grenache might be linked to its sensitivity to ABA and xylem sap pH acclimation. Photosynthetic recovery is an important competitive advantage of any species; thus, the observed delay can be seen as a disadvantageous behavior. However, this delay might be necessary to assure that xylem transport capacity is restored to its maximum prior to an increase in transpiration demand. It is imperative to reconsider the way we represent recovery from assessing it in terms of water potential to looking at it from the perspective of time passing.

Although in this study we did not assess hydraulic losses due to tension, applied stress was shown to cause embolism in grapevine (Brodersen et al. 2013, Pratt et al. 2020, Brodersen et al. 2018, Tombesi et al. 2014). Furthermore, it has been shown that recovery processes resulting in the restoration of hydraulic capacity require both energy and time to utilize the sudden occurrence of high water potential (Salleo et al. 2004, Secchi and Zwieniecki 2016, Savi et al. 2016, Trifilò et al. 2017). As drought decreases photosynthetic output and growth, consequently it is thought that the NSC storage pool may initially increase due to a reduction in sink activities but subsequently decrease due the expenditure required to maintain metabolic activity (Trifilo et al. 2017). It might be expected that such behavior would be more pronounced in SDD as a slow decrease in plant water potential would allow more time between the halting of growth and total stomata shutdown, while in FDD both growth and stomata shutdown may occur almost simultaneously and no accumulation should be detected. Grenache indeed increased soluble sugar and starch contents under SDD conditions and did not change sugar content under FDD conditions even if an increased in starch level was observed. It is assumed that the restoration of xylem functional capacity post stress-exposure requires a pH driven accumulation of sugars in xylem sap, which creates an osmotic

gradient that stimulates embolism recovery (Salleo et al. 2004, Secchi and Zwieniecki 2016). Such dependency has been previously observed and further supports the notion that under natural drought conditions the pH of xylem sap stimulates an efflux of soluble sugars to the xylem (Secchi et al. 2017). Interestingly, during SDD, this accumulation of sugar in sap was imperceptible; however, during recovery there was a significant increase which was associated with a drop in pH (Fig. 4). Nevertheless, this increase only persisted for a few days. In FDD no significant changes in xylem sap soluble sugar levels were detected and no relationship between sap pH and SC concentration was present. This differential response between SDD and FDD may suggest that SDD results in physiological preparations aimed at reinstating their hydraulic system while FDD (most likely not a realistic drought treatment) can result in artifactual responses that may not facilitate full physiological recovery. Taken together, it seems that the length and rate of drought stress affects xylem sap soluble sugar concentration such that longer and slower stress stimulates processes associated with recovery from embolism, while fast stress progression may hinder physiological preparations for recovery.

Conclusions (consult schematics presented Fig. 8)

- In the case of Grenache isohydric and anisohydric behavior are facultative responses that can be linked to the rate of drought progression with isohydric behavior protecting plants from a sudden increase in tension, while anisohydric response can be linked to a more gradual tension increase that promotes maintenance of photosynthetic activity.
- Stress progression rate affects xylem sap ABA concentration and sensitivity of stomata to ABA with high concentrations and lower sensitivity observed in FDD and low concentrations and high sensitivity in SDD.
- Post-stress recovery occurs in two phases: (1) fast (hours) recovery of water potential and (2) slow (days) yet continuous recovery of stomatal conductance. Recovery rate was independent from the stress progression rate and could be linked to lingering ABA concentrations in xylem sap and respective sensitivities.

- Concentration of stem NSC was minimally affected by stress progression rates. However, xylem sap soluble sugar content increased in SDD in correspondence to lower pH, suggesting that slow developing stress might prime plants for restoring hydraulic capacity.
- The differential response between FDD and SDD, reflected in levels of xylem sap ABA concentration, pH and NSC underlines the importance of applying a drying method that best simulates the timing of naturally occurring drought within the studied system. However, the similarities in the major recovery parameters (water potential and g_s) suggest the method of stress application is less important the rate of drought recovery although the nuances may be different.

Author contributions

CM and JO contributed equally and should be considered first authors. CM and JO planned and designed the research with assistance of FS and MAZ. CM, JO, GT, SC and FS performed the physiological and chemical experiments. MGR conducted the ABA quantification. CM, JO, AS, MAZ and FS contributed to the analyses and discussion of data. JO, CM wrote first version of the manuscript with assistance of FS and MAZ. All authors contributed to final revision. MAZ and FS contributed equally.

Acknowledgements

Francesca Secchi gratefully acknowledges funding from Ateneo CSP/2016 Project (University of Turin). The authors wish to thank Tiziano Strano for grapevines maintenance.

References

Allen CD, Macalady AK, Chenchouni H, Bachelet D, McDowell N, Vennetier M, Kitzberger T, Rigling A, Breshears DD, Hogg EH, Gonzalez P, Fensham R, Zhang Z, Castro J, Demidova N, Lim JH, Allard G, Running SW, Semerci A, Cobb N (2010) A global overview of drought and heat-induced tree mortality reveals emerging climate change risks for forests. Forest Ecology and Management 259(4): 660-684

Anderegg WRL, Kane JM, Anderegg LDL (2013) Consequences of widespread tree Mortality triggered by drought and temperature stress. Nature Climate Change 3(1): 30-36

Blackman CJ, Brodribb TJ, Jordan GJ (2009) Leaf hydraulics and drought stress: response, recovery and survivorship in four woody temperate plant species. Plant Cell and Environment 32(11): 1584-1595

Blum A (2017) Osmotic adjustment is a prime drought stress adaptive engine in support of plant production. Plant Cell and Environment 40(1): 4-10

Brodersen CR, McElrone AJ, Choat B, Lee EF, Shackel KA, Matthews MA (2013) *In Vivo* Visualizations of Drought-Induced Embolism Spread in *Vitis vinifera*. Plant Physiology 161(4)1820-1829

Brodersen CR, Knipfer T, McElrone AJ (2018) In vivo visualization of the final stages of xylem vessel refilling in grapevine (*Vitis vinifera*) stems. New Phytologist 217(1)117-126

Brodribb TJ, McAdam SAM (2013) Abscisic Acid Mediates a Divergence in the Drought Response of Two Conifers. Plant Physiology 162(3): 1370-1377

Chaves MM, Zarrouk O, Francisco R, Costa JM, Santos T, Regalado AP, Rodrigues ML, Lopes CM (2010) Grapevine under deficit irrigation: hints from physiological and molecular data. Annals of Botany 105(5): 661-676

Coupel-Ledru A, Tyerman SD, Masclef D, Lebon E, Christophe A, Edwards EJ, Simonneau T (2017) Abscisic Acid Down-Regulates Hydraulic Conductance of Grapevine Leaves in Isohydric Genotypes Only. Plant Physiology 175(3): 1121-1134

Cramer GR, Ergul A, Grimplet J, Tillett RL, Tattersall EAR, Bohlman MC, Vincent D, Sonderegger J, Evans J, Osborne C, Quilici D, Schlauch KA, Schooley DA, Cushman JC (2007) Water and salinity

stress in grapevines: early and late changes in transcript and metabolite profiles. Functional & Integrative Genomics 7(2): 111-134

Dal Santo S, Palliotti A, Zenoni S, Tornielli GB, Fasoli M, Paci P, Tombesi S, Frioni T, Silvestroni O, Bellincontro A, d'Onofrio C, Matarese F, Gatti M, Poni S, Pezzotti M (2016) Distinct transcriptome responses to water limitation in isohydric and anisohydric grapevine cultivars. Bmc Genomics 17

Daszkowska-Golec A, Szarejko I (2013) Open or close the gate - stomata action under the control of phytohormones in drought stress conditions. Frontiers in Plant Science 4

Davies WJ, Wilkinson S, Loveys B (2002) Stomatal control by chemical signalling and the exploitation of this mechanism to increase water use efficiency in agriculture. New Phytologist 153(3): 449-460

Domec JC, Johnson DM (2012) Does homeostasis or disturbance of homeostasis in minimum leaf water potential explain the isohydric versus anisohydric behavior of *Vitis vinifera* L. cultivars? Tree Physiol 32(3): 245-248

Franks PJ, Drake PL, Froend RH (2007) Anisohydric but isohydrodynamic: seasonally constant plant water potential gradient explained by a stomatal control mechanism incorporating variable plant hydraulic conductance. Plant Cell and Environment 30(1): 19-30

Frioni T, Tombesi S, Sabbatini P, Squeri C, Lavado Rodas N, Palliotti A, Poni S (2020) Kaolin reduces ABA biosynthesis through the inhibition of neoxanthin synthesis in grapevines under water deficit. International Journal of Molecular Sciences 21(14): 4950

Griesser M, Weingart G, Schoedl-Hummel K, Neumann N, Becker M, Varmuza K, Liebner F, Schuhmacher R, Forneck A (2015) Severe drought stress is affecting selected primary metabolites, polyphenols, and volatile metabolites in grapevine leaves (*Vitis vinifera* cv. Pinot noir). Plant Physiology and Biochemistry 88: 17-26

Hochberg U, Rockwell FE, Holbrook NM, Cochard H (2018) Iso/Anisohydry: A Plant-Environment Interaction Rather Than a Simple Hydraulic Trait. Trends in Plant Science 23(2): 112-120

Ingrisch J, Bahn M (2018) Towards a Comparable Quantification of Resilience. Trends in Ecology & Evolution 33(4): 251-259

Ivanov YV, Kartashov AV, Zlobin IE, Sarvin B, Stavrianidi AN, Kuznetsov VV (2019) Water deficit-dependent changes in non-structural carbohydrate profiles, growth and mortality of pine and spruce seedlings in hydroculture. Environmental and Experimental Botany 157: 151-160

Klein T (2014) The variability of stomatal sensitivity to leaf water potential across tree species indicates a continuum between isohydric and anisohydric behaviours. Functional Ecology

Lavoie-Lamoureux A, Sacco D, Risse PA, Lovisolo C (2017) Factors influencing stomatal conductance in response to water availability in grapevine: a meta-analysis. Physiologia Plantarum 159(4): 468-482

Leyva A, Quintana A, Sanchez M, Rodriguez EN, Cremata J, Sanchez JC (2008) Rapid and sensitive anthrone-sulfuric acid assay in microplate format to quantify carbohydrate in biopharmaceutical products: Method development and validation. Biologicals 36(2): 134-141

Lovisolo C, Perrone I, Hartung W, Schubert A (2008) An abscisic acid-related reduced transpiration promotes gradual embolism repair when grapevines are rehydrated after drought. New Phytologist 180(3): 642-651

Martinez-Vilalta J, Garcia-Forner N (2017) Water potential regulation, stomatal behaviour and hydraulic transport under drought: deconstructing the iso/anisohydric concept. Plant Cell and Environment 40(6): 962-976

Martorell S, Diaz-Espejo A, Medrano H, Ball MC, Choat B (2014) Rapid hydraulic recovery in *Eucalyptus pauciflora* after drought: linkages between stem hydraulics and leaf gas exchange. Plant Cell and Environment 37(3): 617-626

Martorell S, Diaz-Espejo A, Tomas M, Pou A, El Aou-Ouad H, Escalona JM, Vadell J, Ribas-Carbo M, Flexas J, Medrano H (2015) Differences in water-use-efficiency between two *Vitis vinifera* cultivars (Grenache and Tempranillo) explained by the combined response of stomata to hydraulic and chemical signals during water stress. Agric Water Manage 156: 1-9, Article

Marusig D, Tombesi S (2020) Abscisic Acid Mediates Drought and Salt Stress Responses in *Vitis vinifera*-A Review. International Journal of Molecular Sciences 21(22)

McDowell N, Pockman WT, Allen CD, Breshears DD, Cobb N, Kolb T, Plaut J, Sperry J, West A, Williams DG, Yepez EA (2008) Mechanisms of plant survival and mortality during drought: why do some plants survive while others succumb to drought? New Phytologist 178(4): 719-739

McDowell NG, Sevanto S (2010) The mechanisms of carbon starvation: how, when, or does it even occur at all? New Phytologist 186(2): 264-266

McDowell NG, Beerling DJ, Breshears DD, Fisher RA, Raffa KF, Stitt M (2011) The interdependence of mechanisms underlying climate-driven vegetation mortality. Trends in Ecology & Evolution 26(10): 523-532

O'Brien MJ, Leuzinger S, Philipson CD, Tay J, Hector A (2014) Drought survival of tropical tree seedlings enhanced by non-structural carbohydrate levels. Nature Climate Change 4(8): 710-714

Pagliarani C, Casolo V, Beiragi MA, Cavalletto S, Siciliano I, Schubert A, Gullino ML, Zwieniecki MA, Secchi F (2019) Priming xylem for stress recovery depends on coordinated activity of sugar metabolic pathways and changes in xylem sap pH. Plant Cell and Environment 42(6): 1775-1787

Pratt RB, Castro V, Fickle JC, Madsen A, Jacobsen Al (2020) Factors controlling drought resistance in grapevine (*Vitis vinifera*, chardonnay): application of a new microCT method to assess functional embolism resistance. American Journal of Botany 107(4):618-627

Pratt RB, Tobin MF, Jacobsen AL, Traugh CA, De Guzman ME, Hayes CC, Toschi HS, MacKinnon ED, Percolla MI, Clem ME, Smith PT (2021) Starch storage capacity of sapwood is related to dehydration avoidance during drought. American Journal of Botany 108(1):91-101

Rogiers SY, Greer DH, Hatfield JM, Hutton RJ, Clarke SJ, Hutchinson PA, Somers A (2012) Stomatal response of an anisohydric grapevine cultivar to evaporative demand, available soil moisture and abscisic acid. Tree Physiol 32(3): 249-261

Romero P, Botia P, Keller M (2017) Hydraulics and gas exchange recover more rapidly from severe drought stress in small pot-grown grapevines than in field-grown plants. Journal of Plant Physiology 216: 58-73

Ruehr NK, Grote R, Mayr S, Arneth A (2019) Beyond the extreme: recovery of carbon and water relations in woody plants following heat and drought stress. Tree Physiol 39(8): 1285-1299

Sala A, Woodruff DR, Meinzer FC (2012) Carbon dynamics in trees: feast or famine? Tree Physiol 32(6): 764-775

Salleo S, Lo Gullo MA, Trifilo' P, Nardini A (2004) New evidence for a role of vessel-associated cells and phloem in the rapid xylem refilling of cavitated stems of *Laurus nobilis* L. Plant, Cell and Environment 27: 1065-1076

Savi T, Casolo V, Luglio J, Bertuzzi S, Trifilo P, Lo Gullo MA, Nardini A (2016) Species-specific reversal of stem xylem embolism after a prolonged drought correlates to endpoint concentration of soluble sugars. Plant Physiology and Biochemistry 106: 198-207

Schultz HR (2003) Differences in hydraulic architecture account for near-isohydric and anisohydric behaviour of two field-grown *Vitis vinifera* L. cultivars during drought. Plant Cell and Environment 26(8): 1393-1405

Schwalm CR, Anderegg WRL, Michalak AM, Fisher JB, Biondi F, Koch G, Litvak M, Ogle K, Shaw JD, Wolf A, Huntzinger DN, Schaefer K, Cook R, Wei YX, Fang YY, Hayes D, Huang MY, Jain A, Tian HQ (2017) Global patterns of drought recovery. Nature 548(7666): 202

Secchi F, Zwieniecki MA (2012) Analysis of Xylem Sap from Functional (Nonembolized) and Nonfunctional (Embolized) Vessels of *Populus nigra*: Chemistry of Refilling. Plant Physiology 160(2): 955-964

Secchi F, Zwieniecki MA (2014). Down-regulation of PIP1 aquaporin in poplar trees is detrimental to recovery from embolism. Plant Physiology 164: 1789-1799

Secchi F, Zwieniecki MA (2016). Accumulation of sugars in the xylem apoplast observed under water stress conditions is controlled by xylem pH. Plant Cell and Environment 39:2350-2360

Secchi F, Pagliarani C, Zwieniecki MA (2017) The functional role of xylem parenchyma cells and aquaporins during recovery from severe water stress. Plant Cell and Environment 40(6): 858-871

Sharp RG, Davies WJ (2009) Variability among species in the apoplastic pH signalling response to drying soils. Journal of Experimental Botany 60(15): 4361-4370

Shelden MC, Vandeleur R, Kaiser BN, Tyerman SD (2017) A Comparison of Petiole Hydraulics and Aquaporin Expression in an Anisohydric and Isohydric Cultivar of Grapevine in Response to Water-Stress Induced Cavitation. Frontiers in Plant Science 8

Siciliano I, Carneiro GA, Spadaro D, Garibaldi A, Gullino ML (2015) Jasmonic Acid, Abscisic Acid, and Salicylic Acid Are Involved in the Phytoalexin Responses of Rice to *Fusarium fujikuroi*, a High Gibberellin Producer Pathogen. Journal of Agricultural and Food Chemistry 63(37): 8134-8142

Tardieu F, Simonneau T (1998) Variability among species of stomatal control under fluctuating soil water status and evaporative demand: modelling isohydric and anisohydric behaviours. Journal of Experimental Botany 49: 419-432

Tomasella M, Haberle KH, Nardini A, Hesse B, Machlet A, Matyssek R (2017) Post-drought hydraulic recovery is accompanied by non-structural carbohydrate depletion in the stem wood of Norway spruce saplings. Scientific Reports 7: 14308

Tomasella M, Casolo V, Aichner N, Petruzzellis F, Savi T, Trifilo P, Nardini A (2019) Non-structural carbohydrate and hydraulic dynamics during drought and recovery in *Fraxinus ornus* and *Ostrya carpinifolia* saplings. Plant Physiology and Biochemistry 145:1-9

Tomasella M, Casolo V, Natale S, Petruzzellis F, Kofler W, Beikircher B, Mayr S, Nardini A (2021) Shade-induced reduction of stem nonstructural carbohydrates increases xylem vulnerability to embolism and impedes hydraulic recovery in *Populus nigra.* New Phytologist 231(1): 108-121

Tombesi S, Nardini A, Farinelli D, Palliotti A (2014) Relationships between stomatal behavior, xylem vulnerability to cavitation and leaf water relations in two cultivars of *Vitis vinifera*. Physiologia Plantarum 152(3)453-464

Tombesi S, Nardini A, Frioni T, Soccolini M, Zadra C, Farinelli D, Poni S, Palliotti A (2015) Stomatal closure is induced by hydraulic signals and maintained by ABA in drought-stressed grapevine. Scientific Reports 5: 12449

Trifilo P, Casolo V, Raimondo F, Petrussa E, Boscutti F, Lo Gullo MA, Nardini A (2017) Effects of prolonged drought on stem non-structural carbohydrates content and post-drought hydraulic recovery in Laurus nobilis L.: The possible link between carbon starvation and hydraulic failure. Plant Physiology and Biochemistry 120: 232-241

Trugman AT, Detto M, Bartlett MK, Medvigy D, Anderegg WRL, Schwalm C, Schaffer B, Pacala SW (2018) Tree carbon allocation explains forest drought-kill and recovery patterns. Ecology Letters 21(10): 1552-1560

Tyree MT, Sperry JS (1988) Do woody-plants operate near the point of catastrophic xylem dysfunction caused by dynamic water-stress- answers from a model Plant Physiology 88(3): 574-580

Tyree MT, Sperry JS (1989) Vulnerability of xylem to cavitation and embolism. Annual Reviews of Plant Physiology and Molecular Biology 40: 19-38

Yuan WP, Zheng Y, Piao SL, Ciais P, Lombardozzi D, Wang YP, Ryu Y, Chen GX, Dong WJ, Hu ZM, Jain AK, Jiang CY, Kato E, Li SH, Lienert S, Liu SG, Nabel J, Qin ZC, Quine T, Sitch S, Smith WK, Wang F, Wu CY, Xiao ZQ, Yang S (2019) Increased atmospheric vapor pressure deficit reduces global vegetation growth. Science Advances 5(8)

Zargar A, Sadiq R, Naser B, Khan FI (2011) A review of drought indices. Environmental Reviews 19: 333-349

Zeppel MJB, Wilks JV, Lewis JD (2014) Impacts of extreme precipitation and seasonal changes in precipitation on plants. Biogeosciences 11(11): 3083-3093

Zhang YQ, Oren R, Kang SZ (2012) Spatiotemporal variation of crown-scale stomatal conductance in an arid *Vitis vinifera* L. cv. Merlot vineyard: direct effects of hydraulic properties and indirect effects of canopy leaf area. Tree Physiol 32(3): 262-279

Zwieniecki MA, Secchi F (2015) Threats to xylem hydraulic function of trees under "new climate normal' conditions. Plant Cell and Environment 38(9): 1713-1724

Figures

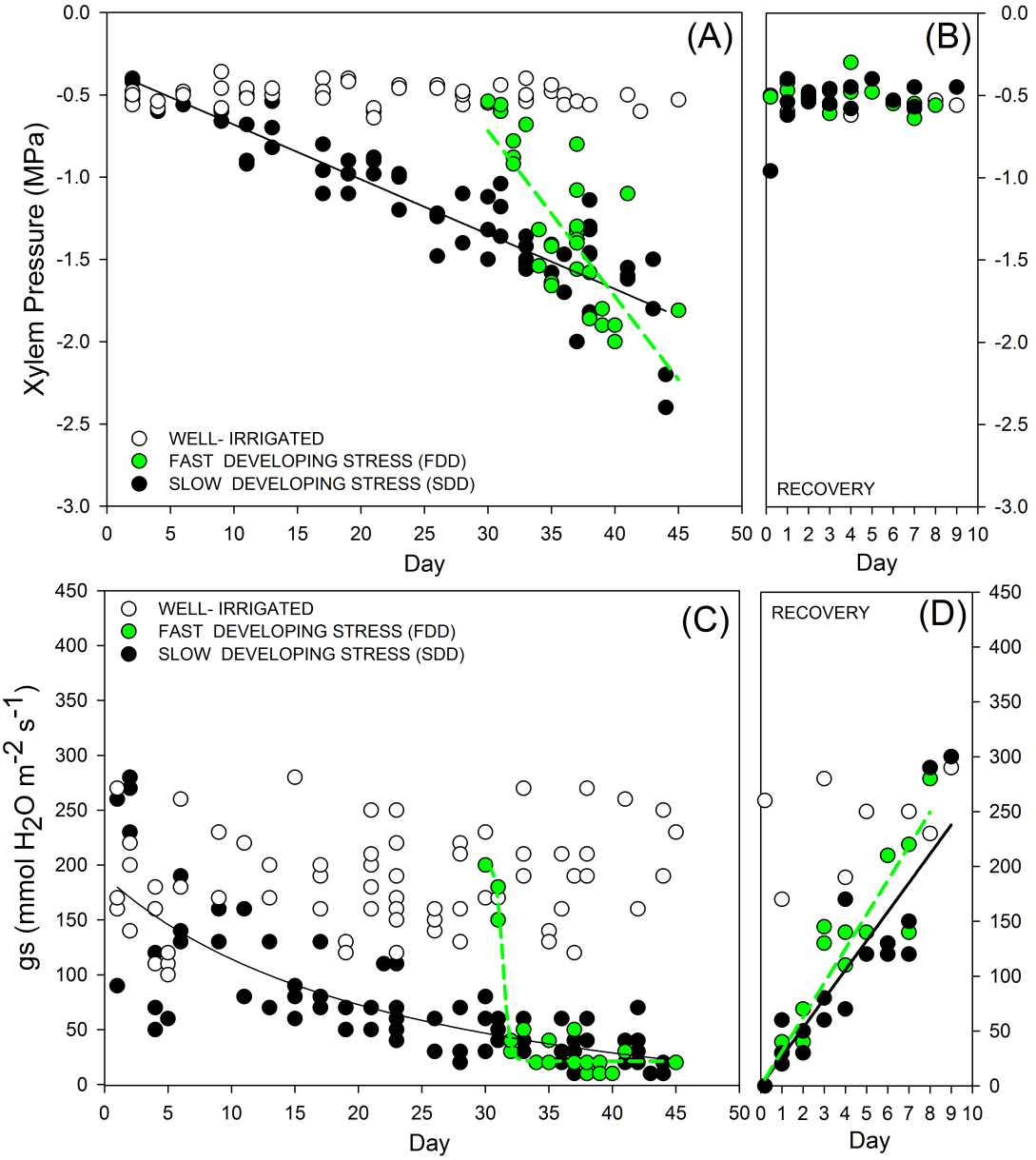

Fig. 1. Temporal dynamics of stem water potential (xylem pressure; a-b) and stomatal conductance (g_s; c-d) during fast developing drought (FDD) and slow developing drought (SDD), and during recovery respectively from FFD and SDD. Each circle represents a plant.

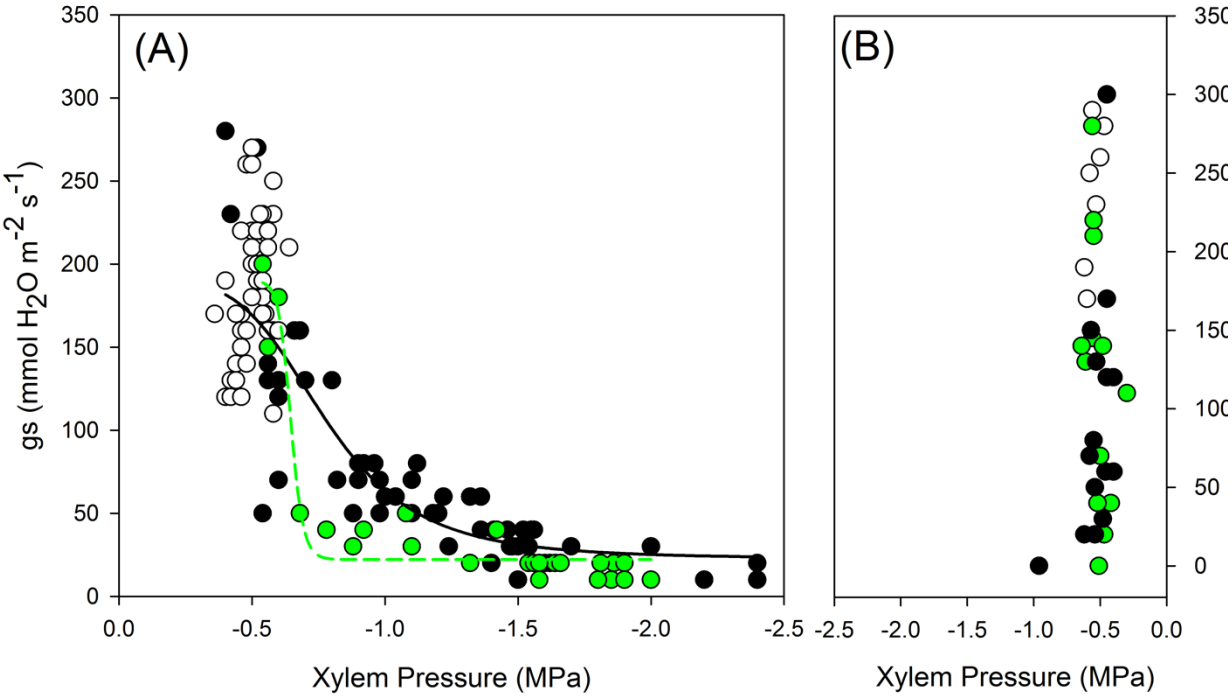

Fig. 2. Stomatal conductance (g_s) in relation to xylem pressure in Grenache plants during (a) fast developing drought (FDD) and slow developing drought (SDD) and during (b) recovery from FDD and SDD. Data were fitted with the four-parameter logistic curves (dose-response curve; black and green lines for respectively SDD and FDD treatment; for more details see Secchi and Zwieniecki, 2014. Parameters that describe curves for the two stressed populations are statistically different (FDD-EC50g_s = -0.645 MPa and SDD-EC50g_s = -0.777 MPa; Paternoster *t* test, $P<0.005$)

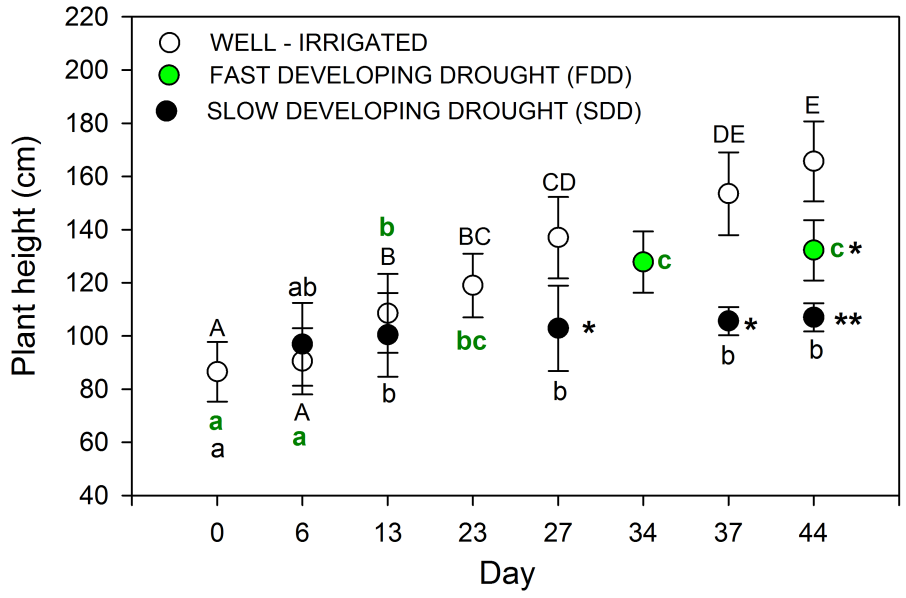

Fig. 3. Temporal plant growth during fast developing drought (FDD; green circles) and slow developing drought (SDD; black circles). White circles denote well-irrigated grapevine plants (CTR). One-way ANOVA tests suggest significant differences among the periods of experiment duration (days) and among the three treatments ($P<0.05$). Among time, letters denote homogeneous groups based on the Fisher LSD method (upper-case letters, differences among well-irrigated plants; lower-case letters, differences among SDD plants and green letters, differences among FDD plants). Asterisks denote significant differences among treatments on the same date. Data are mean values and bars are SE (control: n = 5; SDD and FDD: n = 10).

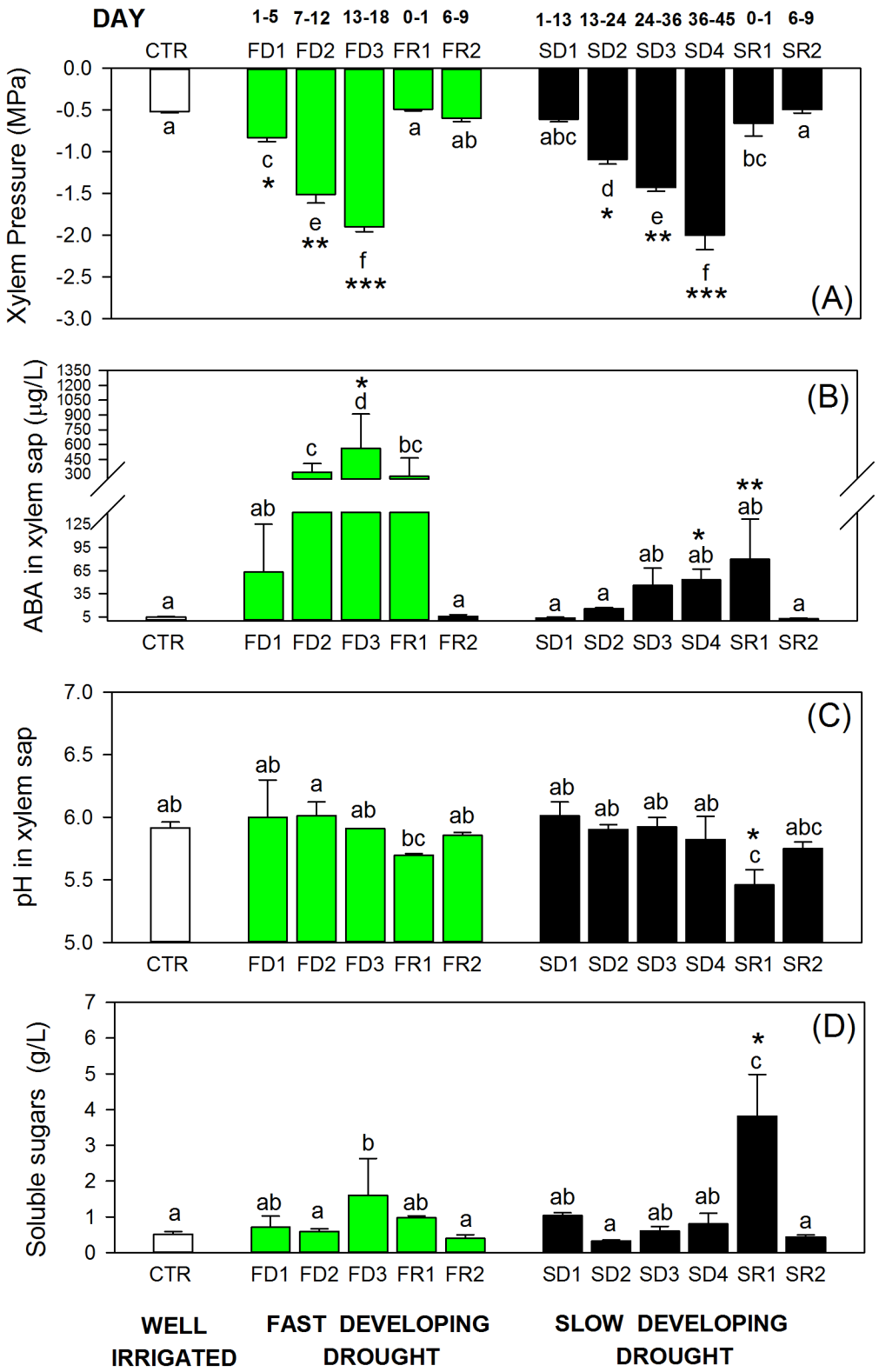
DAY
1-5 7-12 13-18 0-1 6-9
1-13 13-24 24-36 36-45 0-1 6-9
CTR FD1 FD2 FD3 FR1 FR2 SD1 SD2 SD3 SD4 SR1 SR2
Xylem Pressure (MPa)
0.0 -0.5 -1.0 -1.5 -2.0 -2.5 -3.0
(A)
ABA in xylem sap (µg/L)
1350 1200 1050 900 750 600 450 300 125 95 65 35 5
(B)
pH in xylem sap
7.0 6.5 6.0 5.5 5.0
(C)
Soluble sugars (g/L)
7 6 5 4 3 2 1 0
(D)
WELL IRRIGATED
FAST DEVELOPING DROUGHT
SLOW DEVELOPING DROUGHT

Fig. 4. (a) Xylem pressure, (b) abscisic acid (ABA) concentration, (c) pH values and (d) soluble sugar content measured from xylem sap collected from plants exposed to a fast-developing drought (FDD; green bars) and to a slow developing drought (SDD; black bars). White bars indicate average values measured in well-irrigated plants (CTR). One-way ANOVA test suggests significant differences during the imposition of the stresses ($P < 0.05$). Letters denote homogeneous groups based on the Fisher LSD method. Asterisks denote significant differences in SDD and in FDD groups; data are mean values and bars are SE ($n = 3$).

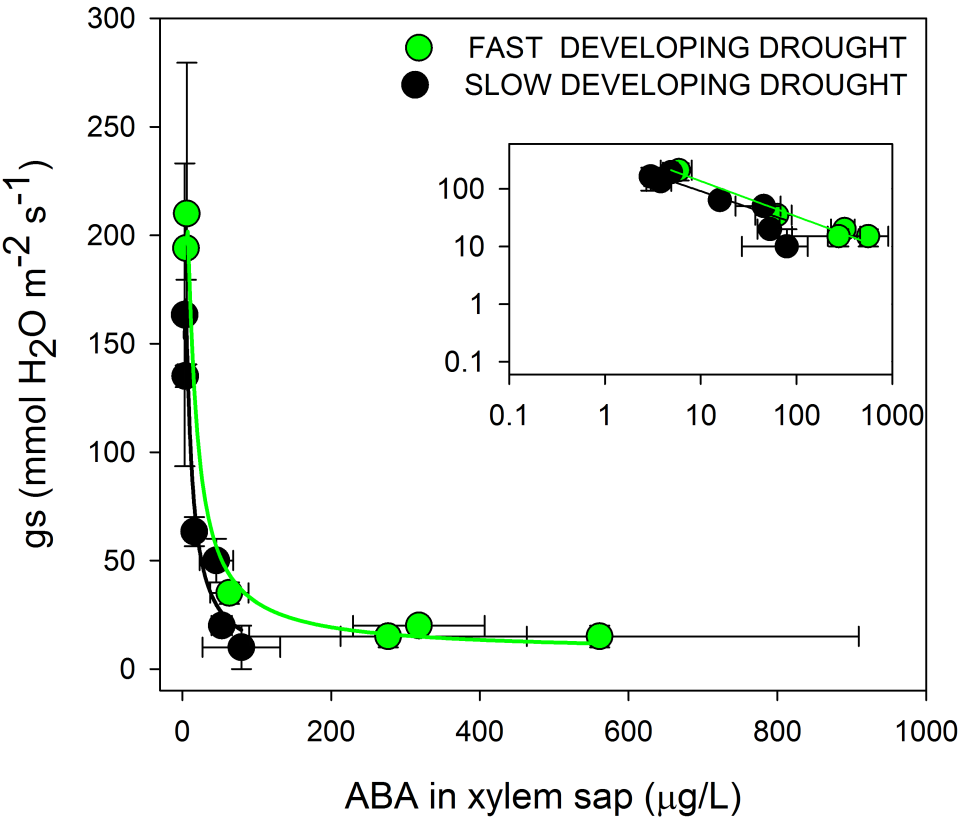

Fig. 5. Relationship between stomatal conductance (g_s) and abscisic acid (ABA) content in xylem sap during fast developing drought (FDD, green circles) and slow developing drought (SDD; black circles). Insets depict stomatal conductance (g_s) *vs* ABA represented with log scale values. Green lines represent the curves obtained for FDD and black lines for SDD treatment. Data are mean values and bars are SE (n = 3).

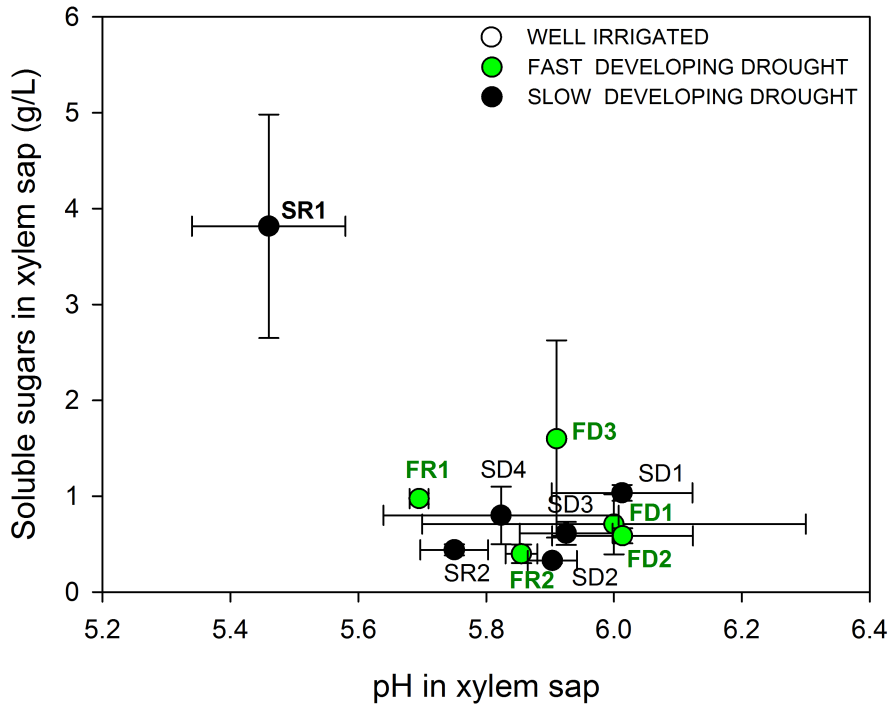

Fig. 6. Xylem soluble sugar content related to pH values during fast developing drought (FDD; green circles) and slow developing drought (SDD; black circles). Data are mean values and bars are SE (n = 3).

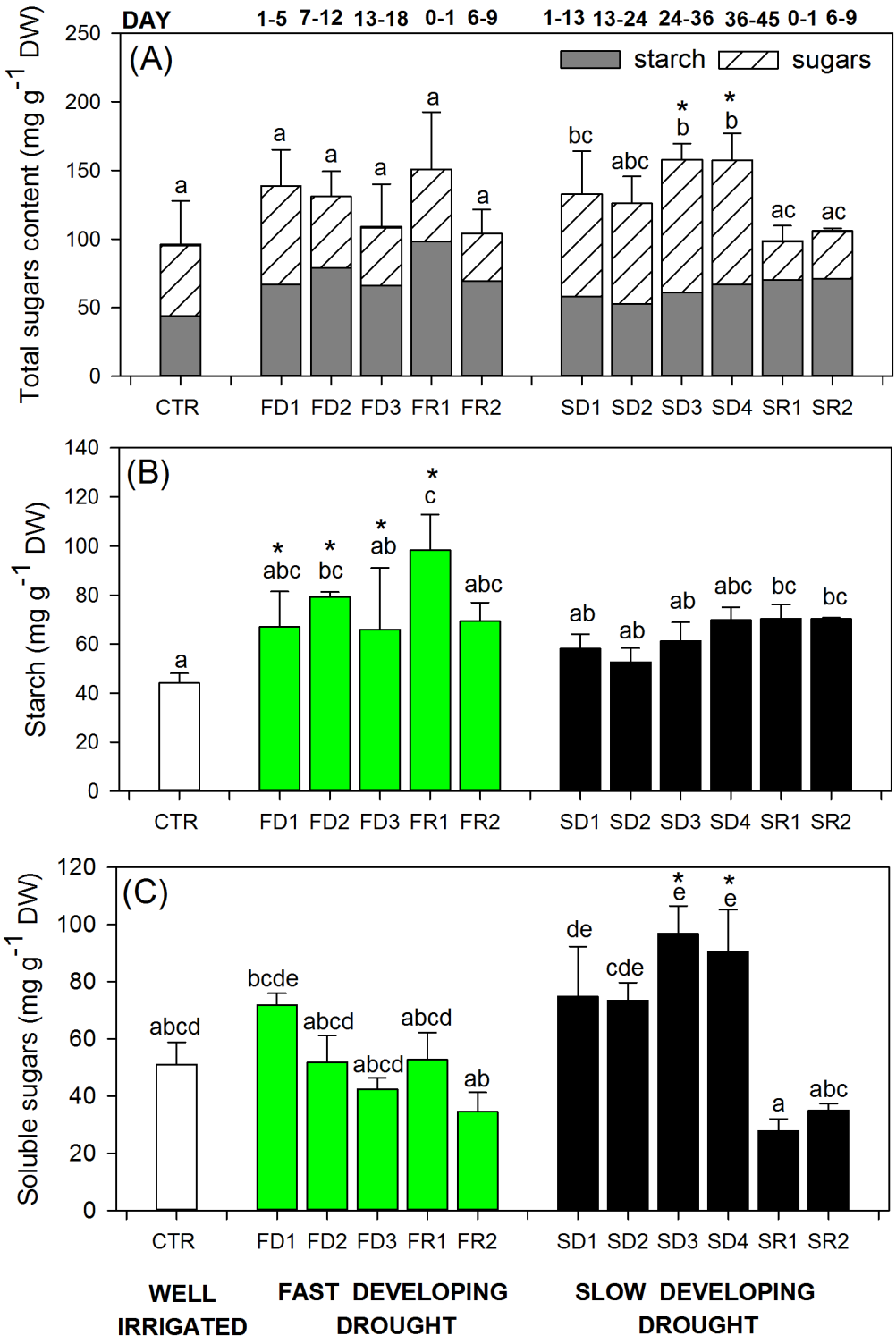

Fig. 7. (a) Total carbohydrates (starch plus soluble sugars), (b) starch content and (c) soluble sugars content measured from stem tissues collected from plants exposed respectively to a fast-developing

drought (FDD; green bars) and to a slow-developing drought (SDD; black bars). White bars indicate average values measured in well-irrigated plants (CTR). One-way ANOVA test suggests significant differences during the imposition of the stresses ($P < 0.05$). Letters denote homogeneous groups based on the Fisher LSD method. Asterisks denote significant differences in SDD and in FDD groups; data are mean values and bars are SE ($n = 3$).

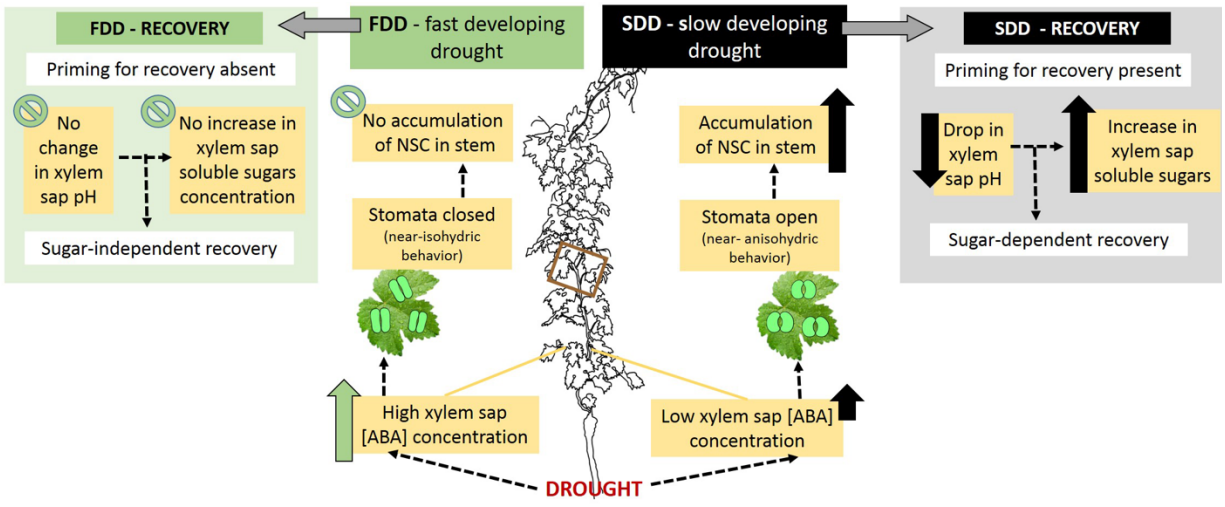

Fig. 8. Schematic illustration of grapevine behaviors under fast-developing drought (FDD; on the left) and slow-developing drought (SDD; on the right) and under recovery from both stresses. Green (FDD) and black (SDD) arrows indicate increasing or decreasing concentration of the measured parameters. Dotted arrows connect the effects derived from exposing plants to the two different rates of stress and the final consequences on recovery. For the details, please refer to the text.

Ch.2 Up in smoke: Assessing the Impacts of Prolonged Fires on Carbohydrate Reserves in Trees

Jessica Orozco[1]*, Paula Guzmán-Delgado[1], Maciej A. Zwieniecki[1]

[1]Plant Sciences, UC Davis, CA USA
[*]Corresponding author jsorozco@ucdavis.edu

Abstract

The global incidence of megafires is on the rise, leading to extensive areas being shrouded in dense smoke for prolonged periods, spanning days or even weeks. By integrating a comprehensive, long-term regional dataset with detailed spatiotemporal satellite data, we present compelling evidence of the pronounced impact of heavy smoke plumes. Our findings show that if smoke occurs during the mid-growing season, it causes a temporary decrease in non-structural carbohydrate stores in plants. Moreover, if smoke disrupts the recovery of these stores before dormancy, it leads to a sustained decline that can impact the entire dormancy period. Our results highlight a previously unrecognized threat that could significantly affect plant health and ecosystem stability at a regional level in both agricultural and natural environments.

Main

Recent years have borne witness to an unprecedented increase in the extent and severity of wildfire activity. Perhaps, nowhere has this growing trend been more salient than in California, where 2020 marked the largest and most destructive wildfire season in the state's recorded history, scorching over 1.5 million hectares of land and enshrouding California in smoke. Wildfire smoke deposits a suite of hazardous compounds, including but not limited to, particulate matter, carbon monoxide, ozone, and aerosol pollutants into the environment that can linger in the atmosphere for days, weeks, or even months [1]. These smoke pollutants not only compromise air quality, which has been linked to a variety of adverse health effects in humans, but they also substantially alter the way sunlight interacts with the environment, upon which plants

depend [2]. Considering that plants rely on light to conduct photosynthesis, any perturbances to the light regime can potentially hamper or amplify photosynthesis, thereby impacting plant growth, long-term productivity and survival [3,4]. In particular, smoke particles can both decrease total solar radiation and enhance diffuse radiation. This dual action may lead to a rise in ecosystem productivity through the "diffuse radiation fertilization" effect at low smoke intensity levels [5,6], while potentially reducing productivity due to a decline in total solar radiation at high smoke levels [7,8] or atmospheric pollutants. Despite the potential consequences, the impacts of long-term natural smoke exposure on plants have been understudied. Conducting broad-scale experiments involving long-term smoke exposure is not feasible, emphasizing the importance of leveraging large natural events to gain a more comprehensive understanding of smoke's impact on plant life.

Plants' response to smoke exposure can be influenced by multiple factors and affect various plant functions. Since a plant's energy reserves, such as non-structural carbohydrates (NSC), form an integral link between photosynthesis and diverse functions like growth, development, defense, phenology, and metabolism, investigating the dynamics of NSC storage can offer valuable insights into the effects of smoke on plants. In all plants, stores are needed to compensate for periods of asynchrony between carbon production and usage, such as day/night cycles, when current assimilate is inadequate to fulfill immediate needs of the plant. In perennial plants, substantial NSC storage is crucial for sustaining extended periods of supply-demand imbalance, such as seasonal dormancy and stress events like droughts or pathogen outbreaks. Consequently, these plants may become highly susceptible to negative consequences if their NSC reserves are impacted by smoke exposure. We have a unique opportunity to assess the impact of prolonged wildfire smoke on NSC reserves in four major tree species, both in natural and orchard environments, by coupling a long-term NSC dataset ('Carbohydrate Observatory'; https://zlab-carb-observatory.herokuapp.com/) with the wide coverage and continuous monitoring offered by satellite aerosol detection (MODIS). In this study, we explore the effects of prolonged smoke exposure on trees' carbon reserves by analyzing the concentration of NSC stores over time, comparing periods before and after smoke exposure. **We**

hypothesized that prolonged exposure to high intensity smoke reduces NSC stores due to its impact on photosynthetic activity.

Aerosol Optical Depth (AOD) is a measure of the amount of atmospheric aerosols, such as dust, smoke, and pollution, that is present in a column of air. Specifically, AOD is a measure of the extent to which aerosols prevent the transmission of light through the atmosphere. To assess the intensity of the wildfire smoke in California's Central Valley (CV), we created a 20-year timeseries comprising of monthly average AOD data. On average, the yearly AOD level is approximately 0.151. However, both September 2020 and August 2021 stand out as anomalies, recording exceptionally high mean optical depth values of 0.598 (Fig. 1a). These increased Aerosol Optical Depth (AOD) values coincided with a surge in burned areas surrounding the Central Valley (CV). (Fig. 1b). The topographical features of the CV, combined with the location of the fires around it, led to persistent large-scale smoke plumes blanketing the valley (Fig. 1d) throughout September 2020 and August 2021 making them the most smoke-polluted months in the last 20 years (Fig. 1a).

Our historical data, which spans three years (2018-2022), includes NSC concentrations in twigs of three major Californian horticultural species—*Prunus dulcis* (almond; accounting for 80% of global almond production), *Pistacia vera* (pistachio;70%), and *Juglans regia* (walnut; 30%)—as well as one iconic, endemic species, *Quercus lobata* (oak), all of which are present in the CV. This dataset allows us to examine the impact of the natural smoke exposure "experiment". We analyzed the NSC content for four consecutive months—September, October, November, and December—for two years prior to the anomalous fires (2018 and 2019) and the 2020 and 2021 and post anomalous fires in 2022. Interestingly, we observed a marked difference in the effects of smoke exposure in August compared to those in September. Specifically, we found no immediate impact of AOD on the concurrent levels of NSC (Fig. 2; farm-level, non-standardized data for each species is presented SI Fig 1 to 4) following August smoke, with the exception of bark soluble sugar content. This exception may indicate a reduced capacity for acquiring stores due to an immediate local decreased supply of photosynthates. During the smoke event of September 2020 (Fig. 3; please see SI Fig 5 to 8 for farm-level, non-standardized data for each species), we also did not identify any immediate

effect on carbohydrate reserves. However, while we did not detect any immediate influence on the carbohydrate reserves, soluble sugar levels in October were significantly corelated with September AOD in both bark and wood. This trend continued into November with the addition of a significant reduction of starch levels in wood. By December, the impact of AOD on stores was evident in both the starch content of wood and bark, as well as in the soluble sugar content found in wood (Fig. 3). Our findings indicate that the effect of dense smoke during the mid-growing season (August) on tree reserves is transient, affecting only soluble sugars in the transport tissue (bark). However, the presence of dense smoke during the accumulation of reserves for dormancy (September) has a persistent and dynamic impact. Initially, we observed a reduction in soluble sugar content in October and November across both bark and wood. This was followed by a shift in December, where the decline was noticed in both starch and sugar content, but exclusively in the wood. This study unveils a first-of-its-kind relationship between the prolonged exposure of trees to smoke and the subsequent reduction in their non-structural carbohydrate (NSC) reserves. It provides evidence that smoke exposure during mid-growth is transient, allowing plants to recover before entering dormancy. However, when there's a lack of photosynthate replenishment prior to dormancy, the impacts can be long-lasting. It is difficult to assess the direct cause of the reduced stores in twigs following smoke exposure. This reduction may be related to a decrease in photosynthetic supply, which could stem from several factors: the direct impact of smoke on photosynthetic activity via a reduction in net radiation, changes in light quality (such as increased scattering of red light and attenuation of blue light), or the direct impact of smoke particles on leaf health. To evaluate possibility of the direct impact of smoke exposure on access to CO_2, we analyzed the $\delta^{13}C$ values of all four species on pooled samples from 2019 and 2020 for September, October and December (Fig. 4). Simultaneous pairwise comparisons using Tukey's HSD test revealed that the $\delta^{13}C$ values of all four species (*P. dulcis*, *Q. lobata*, *P. vera* and *J. regia*) were significantly higher in 2020 compared to 2019 ($t(67) = -9.723$, $p < .0001$, Fig. 4). Our findings indicate that in 2020, plants demonstrated reduced discrimination for ^{13}C, suggesting that the decline in NSC content may be primarily attributed to the impact of smoke on net photosynthesis. This effect may arise from decreased stomatal activity, characterized by reduced duration or aperture of stomatal opening, or

alternatively, from a potential simultaneous decline in metabolic activity [9]. Smoke pollutants, such as ozone (O_3), can negatively impact photosynthesis by causing oxidative damage to plant cells and reducing photosynthetic efficiency[10]. Additionally, alterations in the blue/red light ratio have been associated with reduced stomatal opening [11].Nevertheless, other factors cannot be ruled out, such as the direct clogging of stomata by soot particles or the influence of smoke exposure on plant water status and subsequent changes in soil moisture levels.

The analysis of megafires' impact on perennial plants presented here demonstrates a reduction in energy stores across all studied species, providing unequivocal evidence that high persistent levels of smoke have a negative impact on plant photosynthetic activity. These findings present a novel, yet unrealized threat to agricultural and natural ecosystems related to the impairment of plants' intrinsic capacity to accumulate adequate reserves prior to dormancy, following exposure to severe smoke. As levels of NSC stored can be linked to species phenology [12], the following year's productivity [13] and ultimately survival [14,15]. The observed impact may not be limited to temperate climatic zones alone, as the levels of smoke detected in this study (monthly average AOD = 0.6) were similar to those observed in Amazonia [16]; however, no analysis of NSC reserves was conducted. It is crucial to acknowledge that the reported impacts were only detected by comparing NSC stores over several years across a large geographical area, utilizing hundreds of measurements underlining the importance and necessity of long-term, large-scale observations for understanding such ecological effects.

Materials Methods

Study area

Non-structural carbohydrate and aerosol optical depth data was gathered from 673 farms and 12 oak sites within California's Central valley, an area encompassing 47,000 km^2. Its Mediterranean climate means that the warmest and driest periods coincide during the summer and are conducive to wildfires. In fact, the greatest risk of severe fires occurs toward the end of summer and into fall, from July to October, with activity peaking in September [17].

Satellite Aerosol Optical Depth data

The dataset considered for this study was limited to the Central Valley (CV). The datasets considered for this study, were retrieved from MODIS instrument onboard the Terra platform which overpasses the study area twice a day. We employed the Aerosol Optical Depth (AOD) spectral band at 470 μm product from the Multi-angle Implementation of Atmospheric Correction (MAIC) (Collection 6 Level 2) combined from the Moderate Resolution Imaging Spectroradiometer (MODIS) Terra and aqua. The collection has a 1km spatial resolution and a has a quality assurance confidence screened level-2 pixel-level data. To estimate smoke levels, daily AOD over land were averaged monthly for each pixel in CV and then averaged that over CV. MODIS AOD retrievals are limited to cloud-free pixels, and errors in cloud screening may impact the AOD estimate. The MODIS aerosol cloud mask uses the standard deviation of reflectance in sets of pixels to remove cloudy pixels, which increase spatial variability.

Non-structural carbohydrates (NSC)

Non-structural carbohydrate contents were analyzed in *Prunus dulcis* (almond), *Pistacia vera* (pistachio), *Juglans regia* (walnut), and *Quercus Lobata* (oak). Briefly ~ 10 cm twig samples were collected at monthly intervals from several hundred locations across CV. The samples were then separated into bark and wood tissues, oven-dried, ground and analyzed for the NSC content (soluble sugars and starch) using the anthrone method (Leyva et al. 2008). Non-structural carbohydrate data is publicly accessible at (https://zlab-carb-observatory.herokuapp.com/).

Carbon- isotope abundance ($\delta^{13}C$)

^{13}C isotope analysis was conducted on 2-5 mg of NSC samples using a PDZ Europa ANCA-GSL elemental analyzer interfaced to a PDZ Europa 20-20 isotope ratio mass spectrometer (Sercon Ltd., Cheshire, UK). $\delta^{13}C$ are expressed relative to the international standards VPDB (Vienna Pee Dee Belemnite).

Statistical analysis

We performed all our statistical analysis using the R programming language [18] .Timeseries anomaly detection was conducted using R package 'anomalize' [19] using an anomaly sensitivity of a = .025. The timeseries analysis consisted of decomposing and analyzing the remainders using the Generalized Extreme Studentized Deviate Test to detect outliers. Furthermore, to facilitate the creation of a comprehensive graph inclusive of all species, we standardized the non-structural carbohydrate (NSC) data for each species, taking into account monthly variations across each year this was followed by a correlation analysis of AOD and standardized NSC was performed using R package 'rstatix' [20]. Finally, for the analysis of Carbon- isotope abundance ($\delta^{13}C$) a best-fit model was generated and an analysis of variance (ANOVA) applied followed by the use of the R package 'emmeans' [21] to test whether each species differed significantly between the years 2019 and 2020 with a post hoc contrast analysis.

Data availability

Non-structural carbohydrate data is publicly accessible at (https://zlab-carb-observatory.herokuapp.com/).

References

1. Yu, P. *et al.* Black carbon lofts wildfire smoke high into the stratosphere to form a persistent plume. *Science* **365**, 587–590 (2019).
2. Aguilera, R., Corringham, T., Gershunov, A. & Benmarhnia, T. Wildfire smoke impacts respiratory health more than fine particles from other sources: observational evidence from Southern California. *Nat. Commun.* **12**, 1493 (2021).
3. Roderick, M. L., Farquhar, G. D., Berry, S. L. & Noble, I. R. On the direct effect of clouds and atmospheric particles on the productivity and structure of vegetation. *Oecologia* **129**, 21–30 (2001).
4. Gilbert, M. E. & Ripley, B. S. The effect of smoke on the photosynthetic gas exchange of Chrysanthemoides monilifera. *S. Afr. J. Bot.* **68**, 525–531 (2002).

5. Mercado, L. M. *et al.* Impact of changes in diffuse radiation on the global land carbon sink. *Nature* **458**, 1014–1017 (2009).

6. Rap, A. *et al.* Fires increase Amazon forest productivity through increases in diffuse radiation. *Geophys. Res. Lett.* **42**, 4654–4662 (2015).

7. Yue, X. & Unger, N. Fire air pollution reduces global terrestrial productivity. *Nat. Commun.* **9**, 5413 (2018).

8. Yue, X. & Unger, N. Aerosol optical depth thresholds as a tool to assess diffuse radiation fertilization of the land carbon uptake in China. *Atmos. Chem. Phys.* **17**, 1329–1342 (2017).

9. Farquhar, G. D., Ehleringer, J. R. & Hubick, K. T. Carbon isotope discrimination and photosynthesis. *Annu. Rev. Plant Physiol. Plant Mol. Biol.* **40**, 503–537 (1989).

10. Felzer, B. S., Cronin, T., Reilly, J. M., Melillo, J. M. & Wang, X. Impacts of ozone on trees and crops. *C. R. Geosci.* **339**, 784–798 (2007).

11. Matthews, J. S. A., Vialet-Chabrand, S. & Lawson, T. Role of blue and red light in stomatal dynamic behaviour. *J. Exp. Bot.* **71**, 2253–2269 (2020).

12. Sperling, O. & Zwieniecki, M. A. Winding up the bloom clock—do sugar levels at senescence determine how trees respond to winter temperature? *Tree Physiol.* (2021) doi:10.1093/treephys/tpab051.

13. Zwieniecki, M. A., Davidson, A. M., Orozco, J., Cooper, K. B. & Guzman-Delgado, P. The impact of non-structural carbohydrates (NSC) concentration on yield in Prunus dulcis, Pistacia vera, and Juglans regia. *Sci. Rep.* **12**, 4360 (2022).

14. McDowell, N. G. *et al.* Mechanisms of woody-plant mortality under rising drought, CO2 and vapour pressure deficit. *Nature Reviews Earth and Environment* **3**, 294–308 (2022).

15. McDowell, N. G. Mechanisms linking drought, hydraulics, carbon metabolism, and vegetation mortality. *Plant Physiol.* **155**, 1051–1059 (2011).

16. Palácios, R. *et al.* Evaluation of MODIS Dark Target AOD Product with 3 and 10 km Resolution in Amazonia. *Atmosphere* **13**, 1742 (2022).

17. Swain, D. L. A shorter, sharper rainy season amplifies California wildfire risk. *Geophys. Res. Lett.* **48**, (2021).
18. The R Project for Statistical Computing. https://www.r-project.org/.
19. Tidy Anomaly Detection. https://business-science.github.io/anomalize/.
20. Kassambara, A. Pipe-Friendly Framework for Basic Statistical Tests [R package rstatix version 0.7.2]. (2023).
21. Lenth, R. V. Estimated Marginal Means, aka Least-Squares Means [R package emmeans version 1.8.5]. (2023).
22. CAL FIRE - California Open Data. https://data.ca.gov/dataset/cal-fire.

Ethics declarations
The authors declare no competing interests.

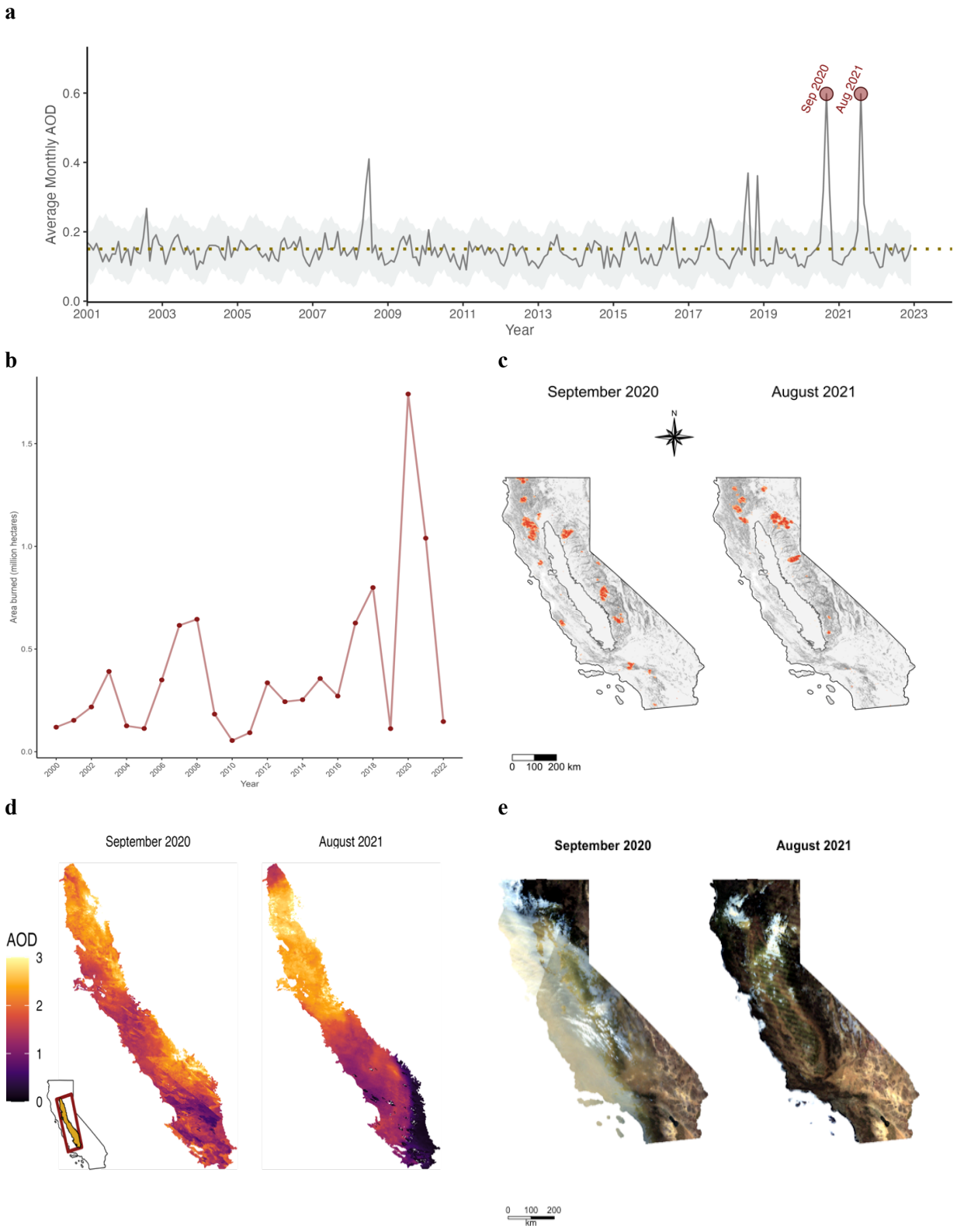
a
Average Monthly AOD
0.0
0.2
0.4
0.6
2001
2003
2005
2007
2009
2011
2013
2015
2017
2019
2021
2023
Year
Sep 2020
Aug 2021
b
Area burned (million hectares)
0.0
0.5
1.0
1.5
2000
2002
2004
2006
2008
2010
2012
2014
2016
2018
2020
2022
Year
c
September 2020
August 2021
N
0 100 200 km
d
September 2020
August 2021
AOD
0
1
2
3
e
September 2020
August 2021
0 100 200
km

Fig 1. Temporal and spatial analysis of the impact of wildfires on the air quality of California Central Valley. **a**) A time series analysis of monthly average aerosol optical depth (AOD) values at 470 nm in California's Central Valley over a 20-year period. The analysis aimed to detect anomalous patterns in the data, which could indicate changes in the amount of aerosols present in the atmosphere. Anomalies are highlighted in the plot by the red circles, indicating significant deviations from the expected trend at an anomaly sensitivity of a = .025. **b**) The total annual burned area in California (2000-2022). **c**) The distribution of the wildfire activity indicated by red markings around the Central Valley; data retrieved from NASA's Fire information for Resource Management System (FIRMS) and the Cal Fire database (2022) [22] **d**) Average monthly values of Aerosol Optical Depth (AOD) across the Central Valley **e**) Visual MODIS representations of the severity and extent of the smoke plumes in California . The images correspond to dates marked by the peak monthly values for Aerosol Optical Depth (AOD). The smoke is observable as feather-like masses appearing in shades of white and off-white.

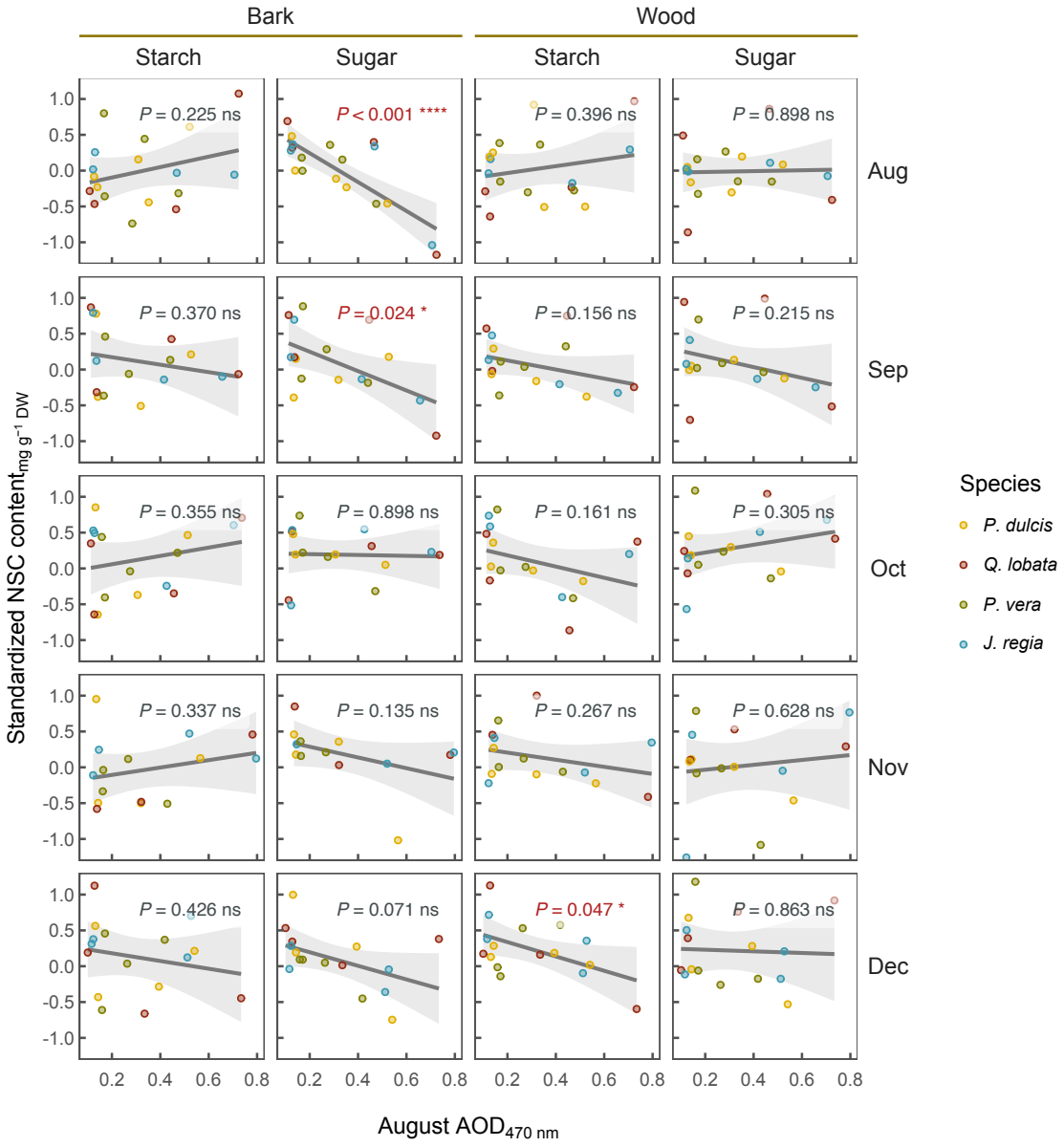

Fig 2. Standardized non-structural carbohydrates (NSC) in four consecutive months plotted against average aerosol optical depth (AOD) in August of the respective year (2018, 2019, 2021 & 2022). The NSC is divided into two components: starch and sugar, and the values are shown for both bark and wood tissues. For every month and NSC type, the linear correlations between standardized NSC and AOD from the four-year analysis period are represented by the solid black line, the gray band represents the 95% confidence interval (n = 16; each respective Pearson's Correlation p-value are displayed in each panel).

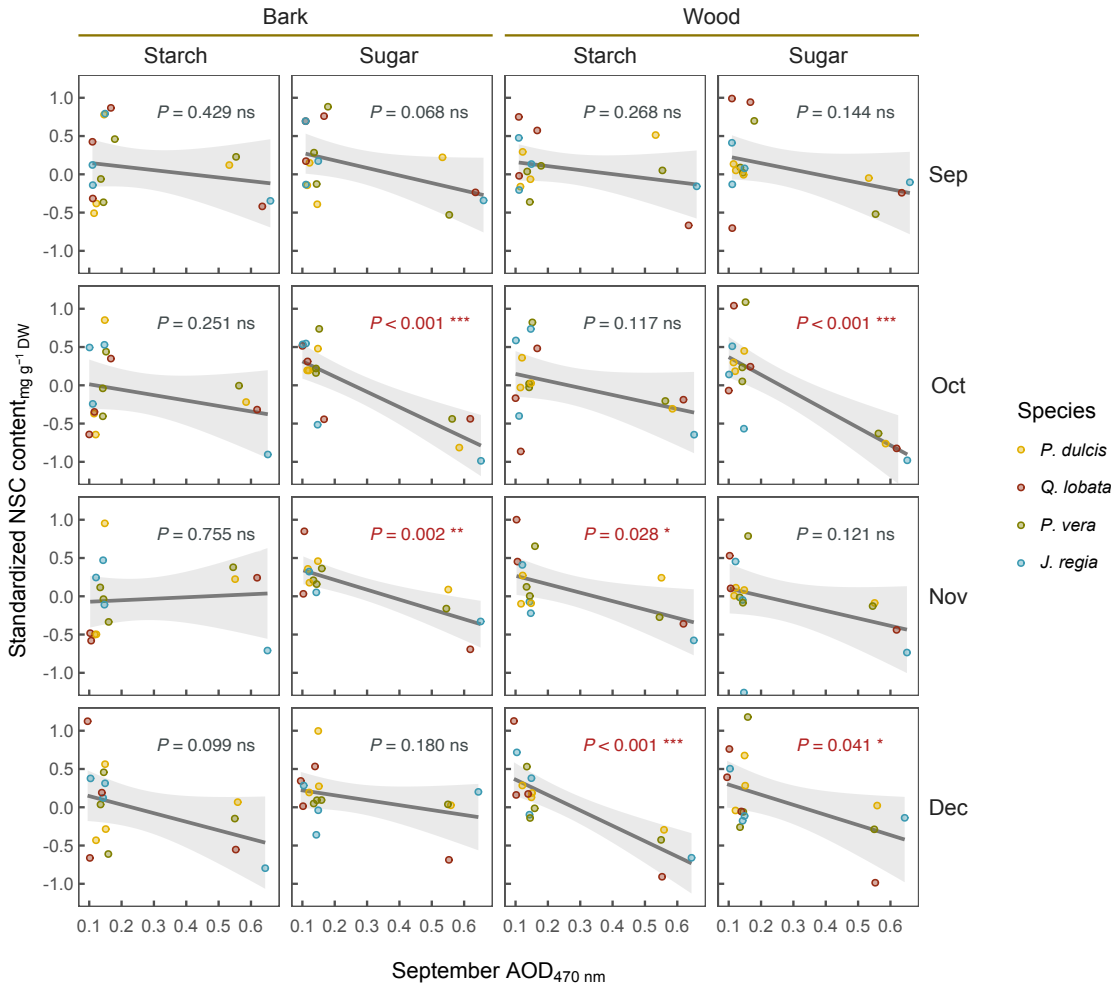

Fig. 3. Standardized non-structural carbohydrates (NSC) in four consecutive months plotted against average aerosol optical depth (AOD) in September of the respective year (2018,2019,2020 & 2022). The NSC is divided into two components: starch and sugar, and the values are shown for both bark and wood tissues. For every month and NSC type, the linear correlations between standardized NSC and AOD from the four-year analysis period are represented by the solid black line, the gray band represents the 95% confidence interval (n = 16; each respective Pearson's Correlation p-value are displayed in each panel)

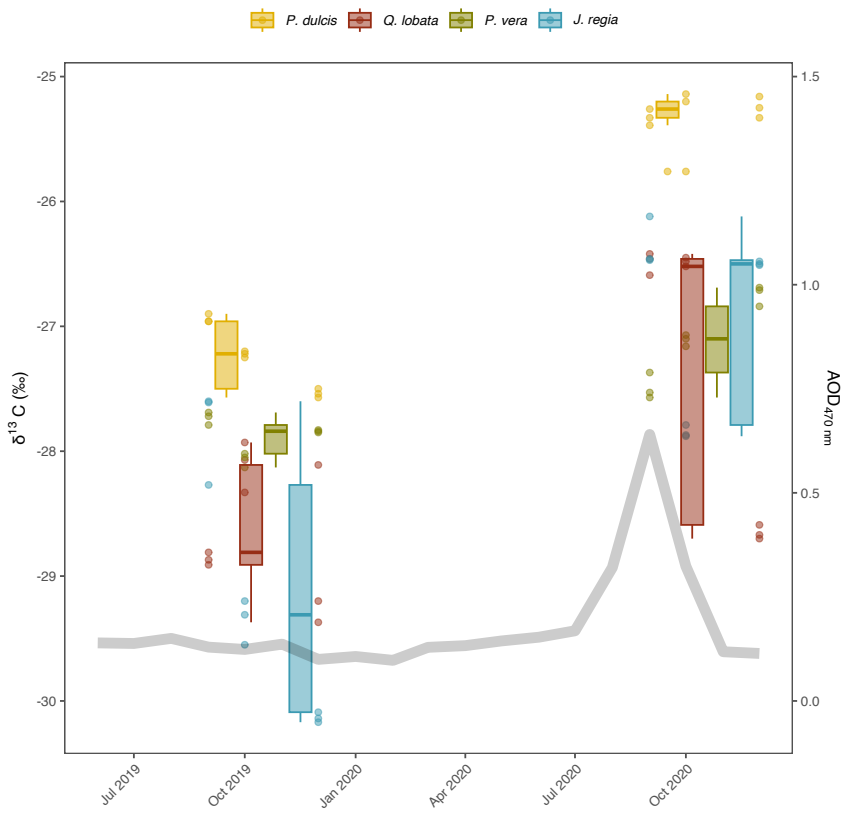

Fig 4. Relative abundance $\delta^{13}C$ in total non-structural carbohydrates for four tree species during the months of September, October, and December in the years 2019 and 2020. The gray band represents the average monthly aerosol optical depth (AOD) for each respective month.

Supplementary Information

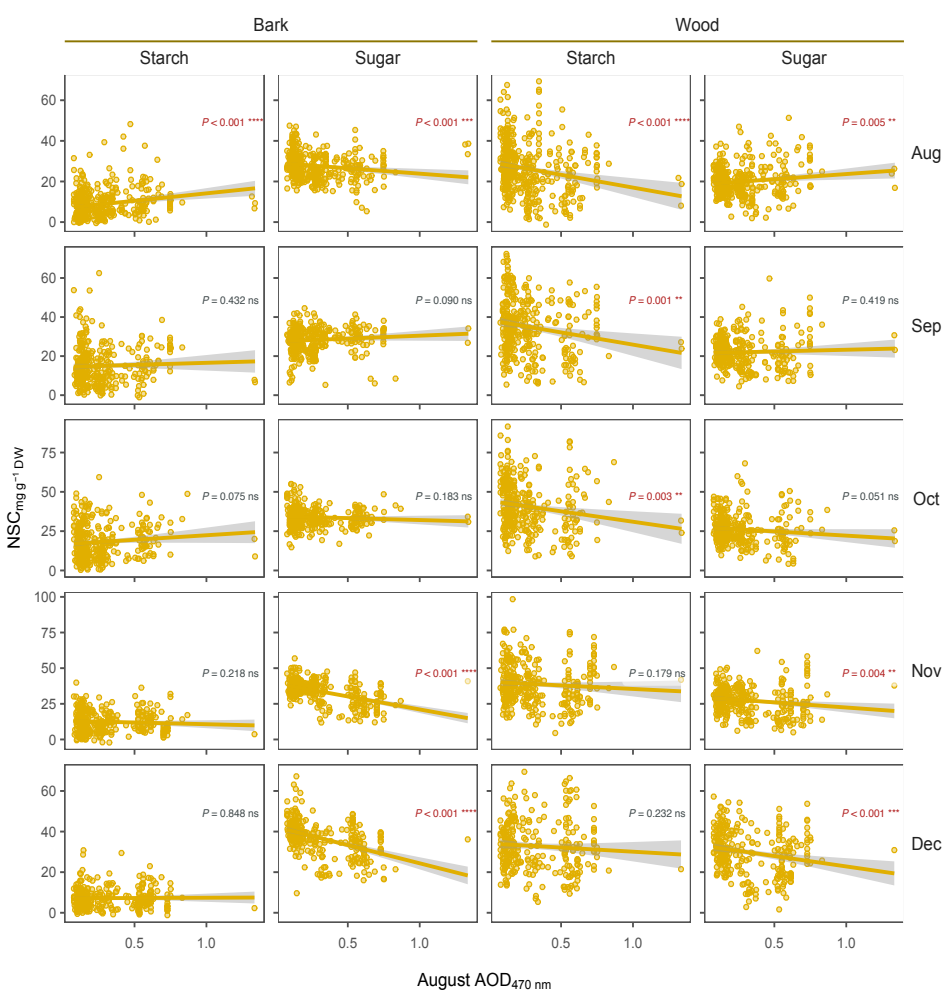

Figure S1. *Prunus dulcis* non-structural carbohydrates (NSC) in four consecutive months plotted against aerosol optical depth (AOD) at each site in August of the respective year (2018, 2019, 2021 & 2022). The NSC is divided into two components: starch and sugar, and the values are shown for both bark and wood tissues. For every month and NSC type, the linear correlations between NSC and AOD from the four-year analysis period are represented by the solid line, the gray band represents the 95% confidence interval (n = 403, 326, 317, 324 and 280 for Aug, Sep, Oct, Nov and December, respectively; each respective Pearson's Correlation p-value is displayed in each panel).

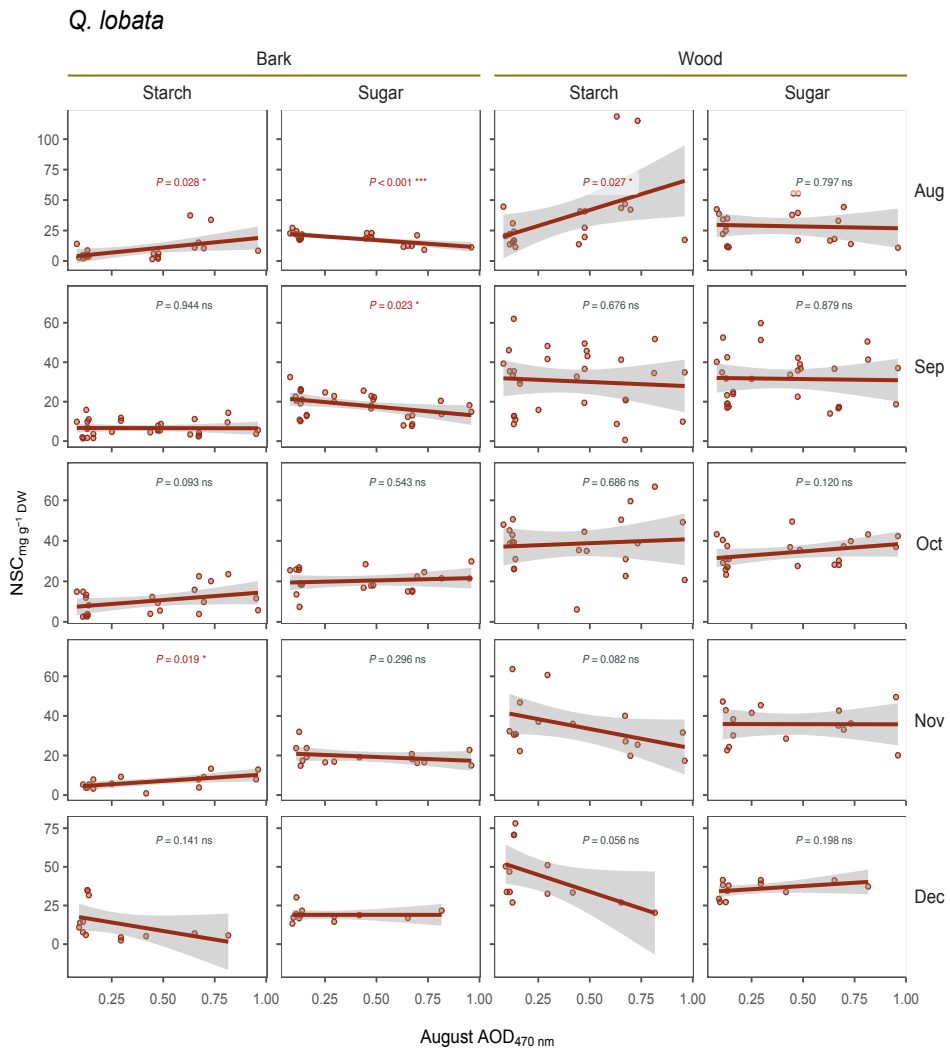

Figure S2. *Quercus lobata* non-structural carbohydrates (NSC) in four consecutive months plotted against aerosol optical depth (AOD) at each site in August of the respective year (2018, 2019, 2021 & 2022). The NSC is divided into two components: starch and sugar, and the values are shown for both bark and wood tissues. For every month and NSC type, the linear correlations between NSC and AOD from the four-year analysis period are represented by the solid line, the gray band represents the 95% confidence interval (n = 21, 30, 22, 15 and 13 for Aug, Sep, Oct, Nov and December, respectively; each respective Pearson's Correlation p-value is displayed in each panel).

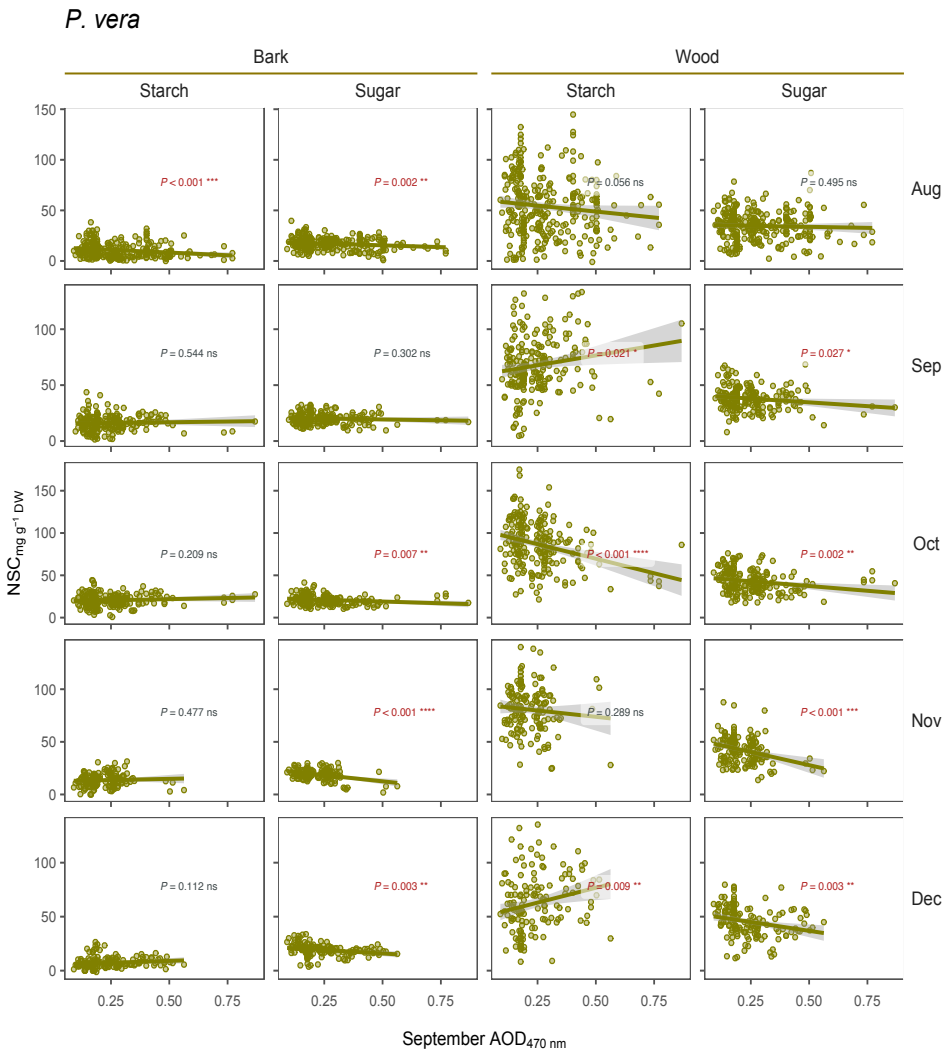

Figure S3. *Pistacia vera* non-structural carbohydrates (NSC) in four consecutive months plotted against aerosol optical depth (AOD) at each site in August of the respective year (2018, 2019, 2021 & 2022). The NSC is divided into two components: starch and sugar, and the values are shown for both bark and wood tissues. For every month and NSC type, the linear correlations between NSC and AOD from the four-year analysis period are represented by the solid line, the gray band represents the 95% confidence interval (n = 288, 199, 199, 150 & 142 for Aug, Sep, Oct, Nov and December, respectively; each respective Pearson's Correlation p-value is displayed in each panel).

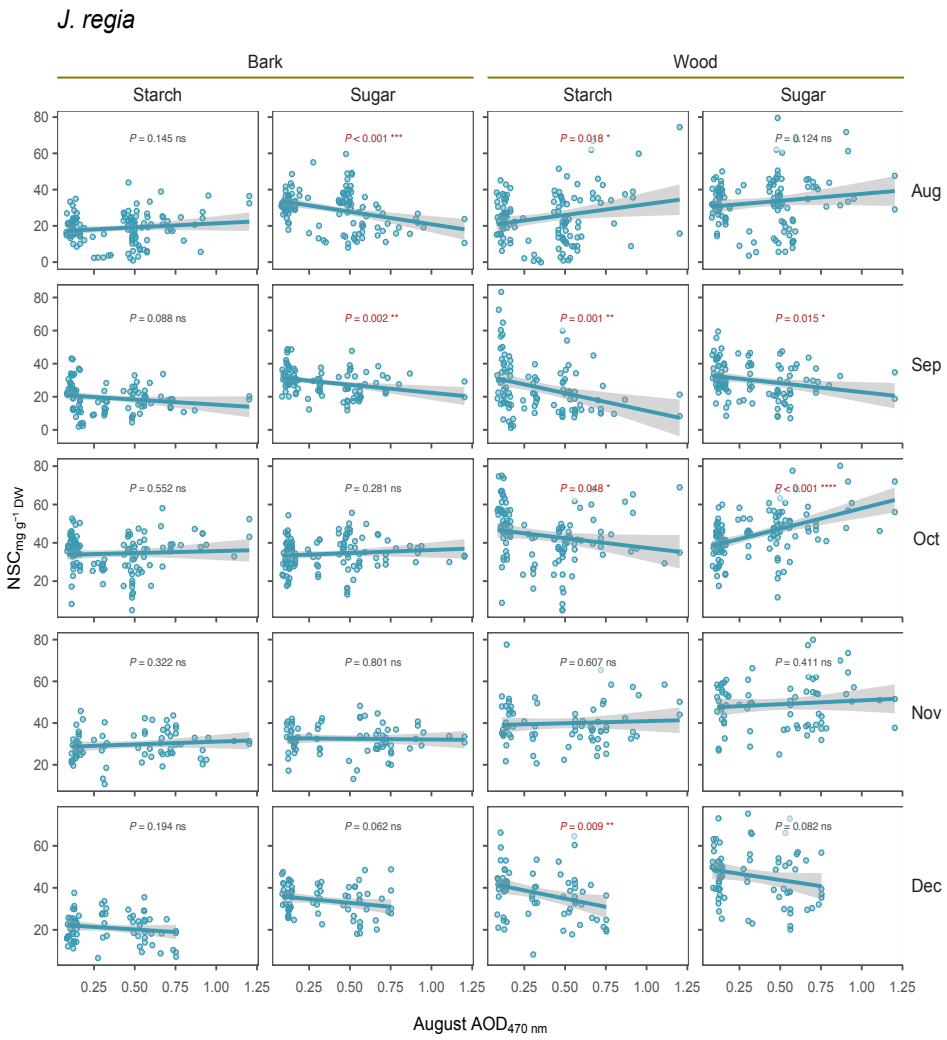

Figure S4. *Juglans regia* non-structural carbohydrates (NSC) in four consecutive months plotted against aerosol optical depth (AOD) at each site in August of the respective year (2018, 2019, 2021 & 2022). The NSC is divided into two components: starch and sugar, and the values are shown for both bark and wood tissues. For every month and NSC type, the linear correlations between NSC and AOD from the four-year analysis period are represented by the solid line, the gray band represents the 95% confidence interval (n = 288, 199, 199, 150 & 142 for Aug, Sep, Oct, Nov and December, respectively; each respective Pearson's Correlation p-value is displayed in each panel).

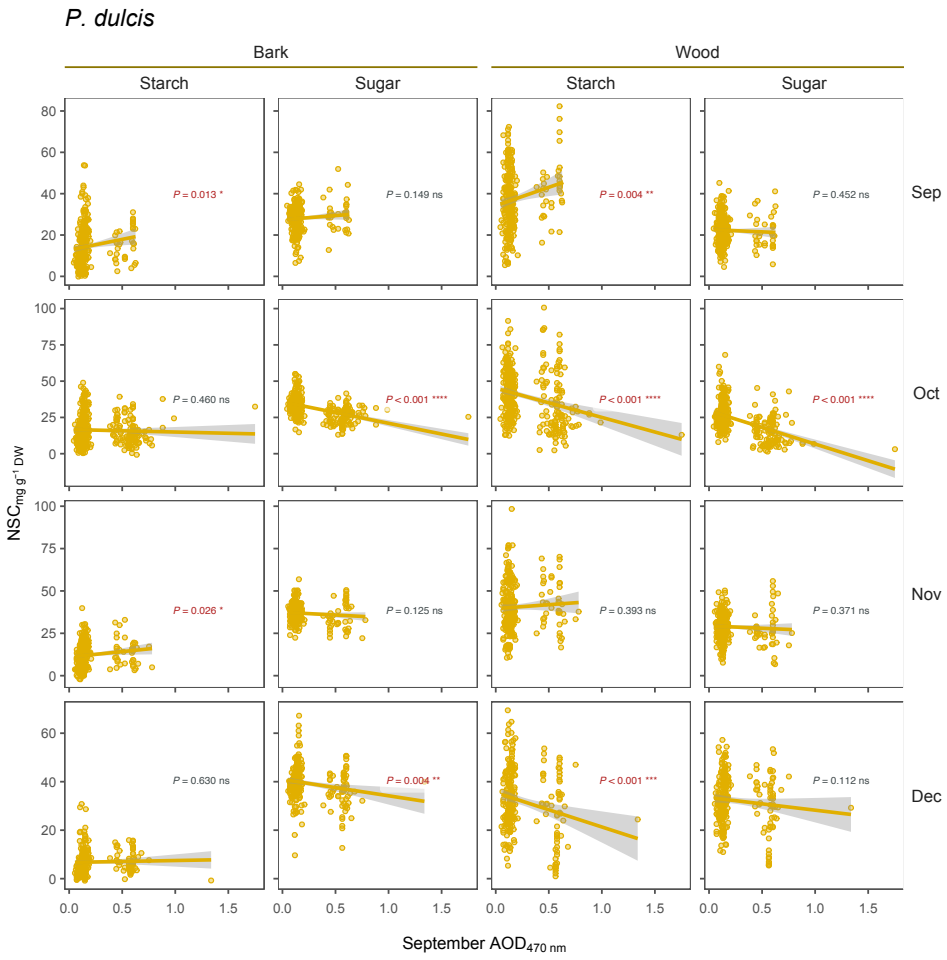

Figure S5. *Prunus dulcis* non-structural carbohydrates (NSC) in four consecutive months plotted against aerosol optical depth (AOD) at each site in September of the respective year (2018, 2019, 2020 & 2022). The NSC is divided into two components: starch and sugar, and the values are shown for both bark and wood tissues. For every month and NSC type, the linear correlations between NSC and AOD from the four-year analysis period are represented by the solid line, the gray band represents the 95% confidence interval (n = 276, 355, 266 and 241 for Sep, Oct, Nov and December, respectively; each respective Pearson's Correlation p-value is displayed in each panel).

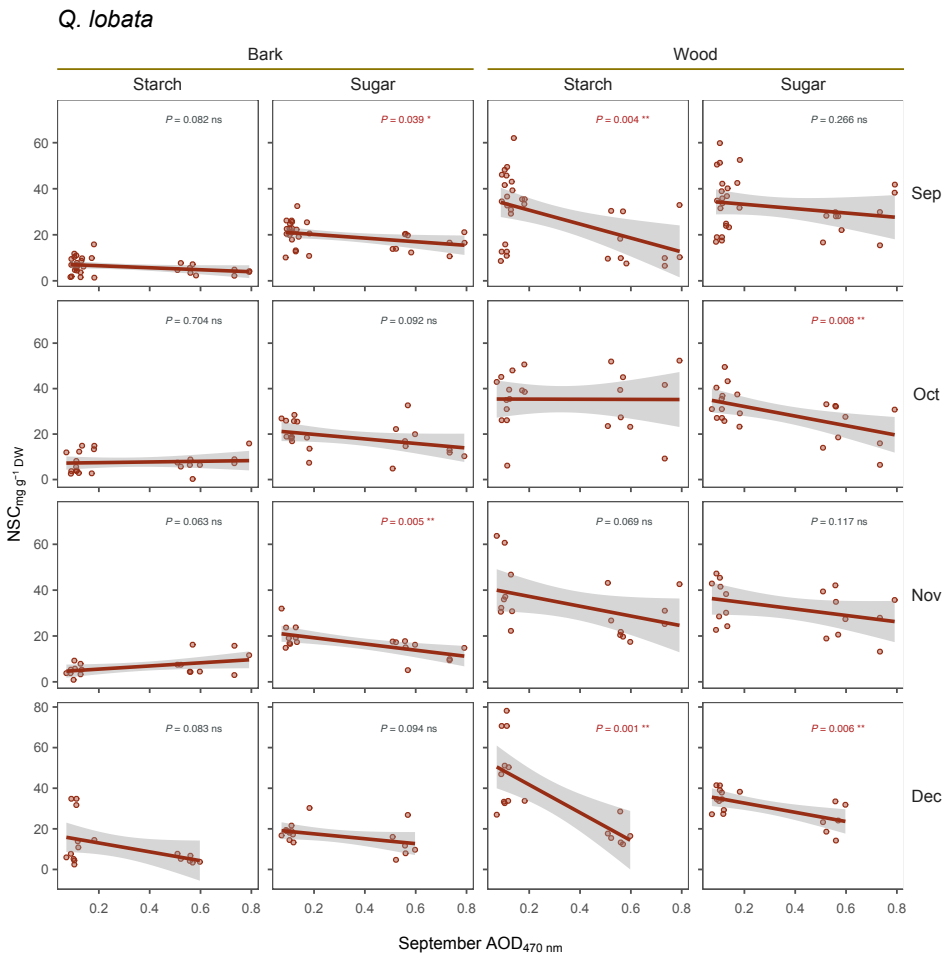

Figure S6. *Quercus lobata* non-structural carbohydrates (NSC) in four consecutive months plotted against aerosol optical depth (AOD) at each site in September of the respective year (2018, 2019, 2020 & 2022). The NSC is divided into two components: starch and sugar, and the values are shown for both bark and wood tissues. For every month and NSC type, the linear correlations between NSC and AOD from the four-year analysis period are represented by the solid line, the gray band represents the 95% confidence interval (n = 27, 18, 18 and 14 for Sep, Oct, Nov and December, respectively; each respective Pearson's Correlation p-value is displayed in each panel).

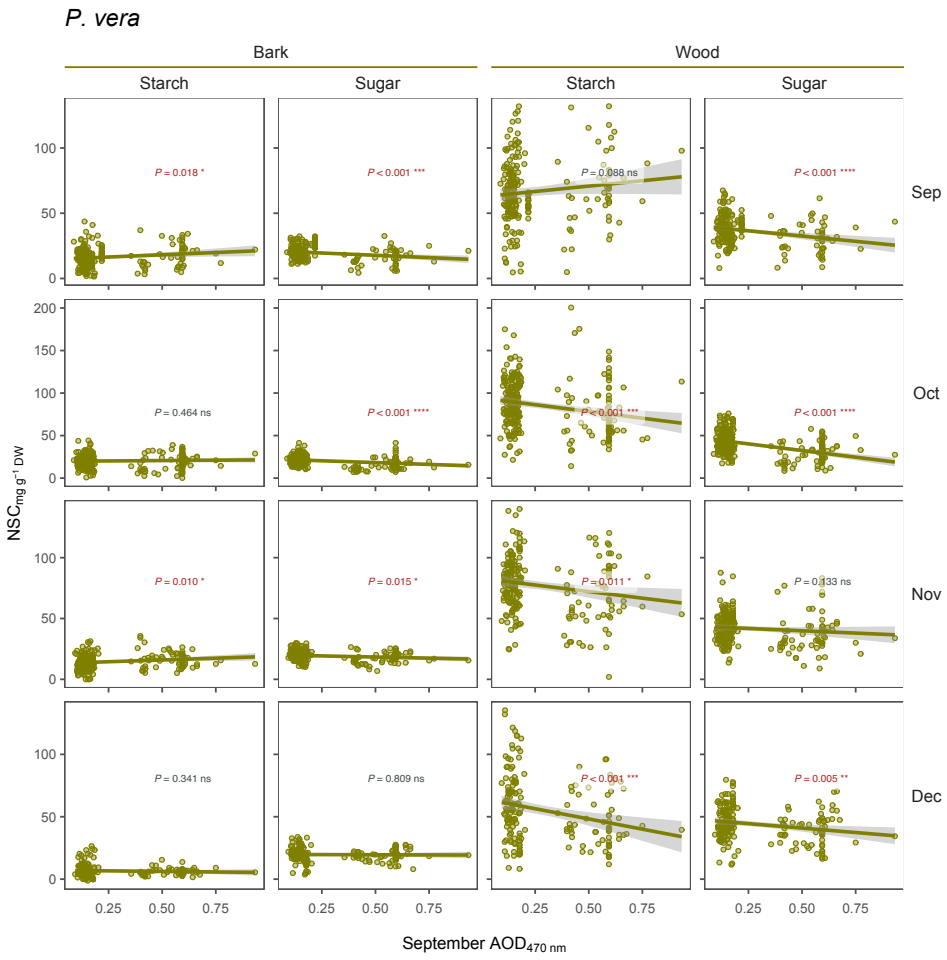

Figure S7. *Pistacia vera* non-structural carbohydrates (NSC) in four consecutive months plotted against aerosol optical depth (AOD) at each site in September of the respective year (2018, 2019, 2020 & 2022). The NSC is divided into two components: starch and sugar, and the values are shown for both bark and wood tissues. For every month and NSC type, the linear correlations between NSC and AOD from the four-year analysis period are represented by the solid line, the gray band represents the 95% confidence interval (n = 211, 258, 206 and 175 for Sep, Oct, Nov and December, respectively; each respective Pearson's Correlation p-value is displayed in each panel).

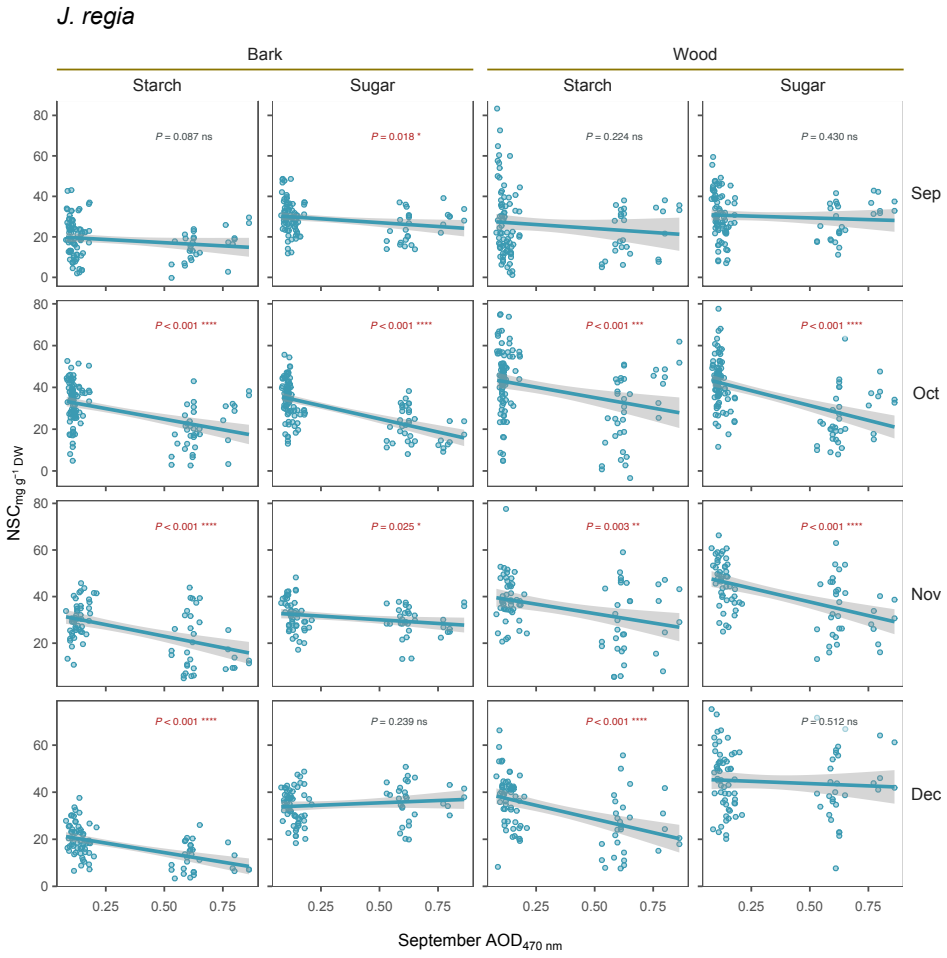

Figure S8. *Juglans regia* non-structural carbohydrates (NSC) in four consecutive months plotted against aerosol optical depth (AOD) at each site in September of the respective year (2018, 2019, 2020 & 2022). The NSC is divided into two components: starch and sugar, and the values are shown for both bark and wood tissues. For every month and NSC type, the linear correlations between NSC and AOD from the four-year analysis period are represented by the solid line, the gray band represents the 95% confidence interval (n = 104, 123, 82 and 87 for Sep, Oct, Nov and December, respectively; each respective Pearson's Correlation p-value is displayed in each panel).

Ch.3 Impacts of Historical and Projected Climate Change on Bloom Timing in California's Almond Orchards

Jessica Orozco[1*], Oren Lauterman[2], Or Sperling[3], Tarin Paz-Kagan[4], and Maciej A. Zwieniecki[1]

1. Plant Sciences, UC Davis, CA USA
2. Department of Mapping and Geoinformation Engineering, Civil and Environmental Engineering, Technion-Israel Institute of Technology, Israel
3. Plant Sciences, ARO-Volcani, Israel
4. French Associates Institute for Agriculture and Biotechnology of Dryland, The Jacob Blaustein Institutes for Desert Research, Ben-Gurion University of the Negev, Sede Boqer Campus, 8499000, Israel.

Abstract

Climate change is expected to impact perennial spring phenology, potentially altering the suitability of land for agricultural purposes. In this study, we investigate the effects of climate change on the bloom timing of almond orchards, focusing on California, the world's leading region for almond production. By analyzing historical climatic data, employing a model that considers daily minimum and maximum temperatures and non-structural carbohydrates, and examining various CMIP6 scenarios, we assess the potential impacts of climate shifts on plant phenology and, consequently, on land suitability for almond farming. Our findings reveal that, within the next 30 years, the land suitable for almond production will not undergo significant changes. However, under unchanged emission scenarios, the available land to support almond orchard farming could decline between 50% to 95% by the end of the century. This reduction corresponds with an early shift in bloom time from the average Day of Year (DOY) 64 observed over the past 40 years to a projected earlier bloom between DOY 28-33 by 2100. These results emphasize the critical role climate shifts have in shaping future land use strategies for almond production in Central Valley, California.

Consequently, understanding and addressing these factors is essential for the sustainable management and preservation of agricultural land, ensuring long-term food security and economic stability in the face of a rapidly changing climate.

Introduction

Climatic conditions can significantly impact the spring phenology of woody perennials and consequently strongly influence species physiology, fecundity, competitiveness, and survival. A synchronous bloom across landscapes in dioecious and self-incompatible species promotes reproductive success, coincides with increased pollinator activity, and is crucial to productivity in horticulture. Numerous phenology observational studies carried out in seasonal climates have explored the influence of local winter temperatures on year-to-year bloom variability and their impact on synchrony [23–25]. An iconic example of synchronous spring bloom is the annual cherry blossom event in Kyoto City. Although the bloom remains synchronous within each year, year-to-year variations in bloom timing, spanning over a month from late March to early May, have been documented for over a thousand years. These variations in bloom timing have been associated with spring temperatures and have been used to partially reconstruct past climate conditions during the blooming period [26,27]. Recent phenology observational studies consistently demonstrate the significant influence of global warming on bloom timing, typically indicating a shift toward earlier blooms in temperate climates [28]. However, only a handful of studies specifically associate bloom synchrony with increasing global temperatures, often showing decreased synchrony [29]. Furthermore, shifts in timing and loss of synchrony can have upstream repercussions on land suitability dynamics by enhancing or restricting the areas that can sustain or promote species survival or their productivity in the case of horticultural systems. Therefore, it is essential to examine the potential impacts of climate change on the spring phenology of long-lived, high-input cropping systems in the upcoming years. Predicting climate's effect on bloom time will help address uncertainties associated with new orchard plantation establishment and ensure the sustainability of these cropping systems.

Winter temperatures throughout the entire period of dormancy affect trees' spring phenology, not just the temperatures experienced in spring. Specifically, an accumulation of chill hours is necessary to initiate a dormancy break in response to spring warming [30,31]. The chill requirement of crops has probably evolved as a protective mechanism against frost damage after premature blooming, which could occur in the rare (less rare considering climate shifts) events of warm winters. Multiple statistical approaches have harnessed the strong correlation between bloom and the accumulation of chill and heat hours. Still, in most cases, empirical methods can only determine the readiness of trees to bloom, not the exact date [23,32]. A more recent and mechanical approach to predicting crop bloom times integrated the "dormancy clock" with the levels and metabolic activity of nonstructural carbohydrates (NSC), such as sugars and starches, which respond to winter temperature. This model predicts bloom time by hourly temperatures from the onset of dormancy until bloom [12,33]. The model also enables the prediction of bloom times in multiple locations, which is crucial in assessing the suitability of an area for horticultural purposes in the future.

The Central Valley in California, USA, is a significant global almond producer, accounting for 80% of the world's almond supply. We postulated that a synchronized bloom of cross-pollinating almond varieties would protect almond reproduction from adverse temperature conditions in spring. An early bloom could compromise fruit set by late frost exposures that would damage the buds or rains that limit bee pollination. Yet, a late bloom can result in pollen inactivity due to exposure to high temperatures (>21°C). Hence, we set to analyze the past and future impact of winter temperatures on the bloom timing of almonds across the Central Valley. We aimed to evaluate the effects of past climate changes on almond spring phenology, and to predict the suitability of the California Central Valley for future almond production by CMIP6 scenarios.

Materials and methods

Temperature data

First, we needed to determine the spatial and temporal variability in California's Central Valley winter temperatures. We used PRISM gridded four-by-four km daily minimum and maximum temperatures for Central Valley, California, focusing on winters ranging from October 15th to April 30th from the fall of 1981 till the spring of 2022 (PRISM Climate Group, Oregon State University, https://prism.oregonstate.edu). Winter average maximum and minimum temperatures were calculated for a period as:

$$\bar{T}_{PRISM\ \max|\min} = \frac{\sum_{15^{th}October(year)}^{30^{th}April(year+1)} \frac{\sum T_{\text{PRISM max}\ |\ min}}{number\ of\ grid\ points}}{number\ of\ days} \qquad Equation\ (1)$$

To predict the influence of climate change on winter temperatures for the years 2050 and 2100, we utilized two CMIP6 models[34], SSP5-8.5 (no emission control) and SSP1-2.6 (emission reduction). This involved adjusting winter minimum and maximum temperatures according to the projected changes in CMIP6 surface air temperatures (ΔT_{SSP}). Specifically, the SSP5-8.5 scenario predicts an increase of 1.6°C and 3.8°C for 2050 and 2100 respectively, while SSP1-2.6 anticipates a rise of 1.1°C for both time points (equation 2; scenarios: SSP5-8.5$\Delta T_{min\cdot max}$, SSP1-2.6 $\Delta T_{min\cdot max}$). Additionally, we added a hypothetical condition where only the maximum temperature increases while the minimum temperature remains constant (as per equation 3; scenarios: SSP5-8.5ΔT_{max}, SSP1-2.6 ΔT_{max}).

$$\bar{T}_{FUTURE\ \max\ |\ \min} = \frac{\sum_{1^{st}October(year)}^{30^{th}April(year+1)} \frac{\sum T_{\text{PRISM max}+\Delta T_{SSP}\ |\ \min+\Delta T_{SSP}}}{number\ of\ grid\ points}}{number\ of\ days} \qquad Equation\ (2)$$

$$\bar{T}_{FUTURE\ \max\ |\ \min} = \frac{\sum_{1^{st}October(year)}^{30^{th}April(year+1)} \frac{\sum T_{\text{PRISM max}+2\Delta T_{SSP}\ |\ min}}{number\ of\ grid\ points}}{number\ of\ days} \qquad Equation\ (3)$$

Predicting historic and future bloom dates

By integrating historical PRISM data with the bloom prediction model[12,33] we generated forecasts for the Day of the Year (DOY) representing the bloom date within each 4x4 km grid across the Central Valley, over a span of 40 years (1982-2022). Furthermore, to anticipate bloom timings for future years, specifically 2050 and 2100, we applied the bloom model in conjunction with the aforementioned CMIP6 temperature adjustments. Moreover, to account for year-to-year variability in winter temperatures, we incorporated data from the four most recent consecutive years (2018-2022). This approach was maintained for each 4x4 km grid across the Central Valley.

Comparing historical bloom predictions with future bloom projections

To assess how the different scenarios (SSP5-8.5$\Delta T_{min \cdot max}$, SSP1-2.6$\Delta T_{min \cdot max}$, SSP5-8.5ΔT_{max}, SSP1-2.6ΔT_{max}) would impact bloom time in comparison to the past (1982-2022) using R Statistical Software (v4.2.2: R Core Team 2022) we constructed a linear regression model where each scenario served as a predictor for bloom date (DOY). This was followed by executing an Analysis of Variance (ANOVA) paired with a post-hoc Dunnett's test contrast analysis.

Results

For the last 40 years, we observed a significant increase of 1.4°C (~ 0.033°C year^{-1}; p = 0.00932; Fig 1) in winter (October 15th – April 30th) mean maximum temperatures, from 17.8°C to 19.2°C. The standard deviation of maximum mean temperature across the Central Valley remained constant at ~0.06°C (Fig. 1b) for 40 years. Mean minimum winter temperature remained almost constant during the last 40-year period, changing only by 0.3°C from 5.6°C to 5.9°C (0.006°C year^{-1}; p=0.532; Fig. 1a). Interestingly, there was a

significant increase in standard deviation from 0.46°C to 0.63°C (p=0.000189; Fig. 1b) of the mean minimum temperature suggesting higher nightly variability.

Our projections of almond bloom dates across California's Central Valley, based on the data from the past 40 years (1982-2022), demonstrated significant variations in bloom dates. On average, the predicted bloom day advanced by 6.5 days in 40 years, shifting from March 7th to March 2nd (on average, trees bloomed on March 5th). The bloom delay corresponds to a change in DOY from 66 to 61 and an average bloom at the 64th DOY. The inter-annual variability in peak bloom, when 70% of blossoms have opened, ranges from February 5th to March 16th (35th to the 75th DOY; Fig. 2a). There is also an annual variability in how bloom is synchronized across California's Central Valley. For instance, in 1985 and 2004, the bloom exhibited a single peak time (DOY 60 and 71, respectively) and spanned ten days across the entire Central Valley, indicating strong synchronicity. On the other hand, in 1982 and 1999, the bloom prediction extended over 25 days without a discernible peak (both DOY 74), demonstrating a high degree of asynchrony (Fig. 2b). In such asynchronous years, there was a solid latitudinal gradient in bloom time, with regional differences between that north and south (Fig. 2c).

We utilized the projected average global temperature increases for 2050 and 2100 from the CMIP6 climate model simulations to assess the effects of future climate shifts on almond bloom time. The climatic projections were based on two distinct scenarios: the first scenario involves a gradual reduction in emissions resulting in limited warming of 1.1°C (SSP1-2.6) for both 2050 and 2100, while the second scenario assumes an unchanged emission pathway with a mean warming of 1.6°C and 3.8°C (SSP5-8.5)[34] for 2050 and 2100, respectively. To estimate the average impact on the bloom DOY while accounting for yearly variability, we applied an average winter temperature increase to both the minimum and maximum daily temperatures ($\Delta T_{min \cdot max}$) to each of four consecutive years (2019, 2020, 2021 and 2022). This time span exhibits inter-annual winter temperature variability while maintaining natural weather patterns. Additionally, following observations in Fig. 1a, we analyzed a rise only in daily maximum temperature (ΔT_{max}) and kept the nighttime temperature constant. Generally, both SSP1-2.6 and SSP5-8.5 models

predicted a significant impact of future climate shifts on bloom time (ANOVA; ($F(6, 63) = 15.8$; $p < 0.0001$). Post-hoc tests using the Dunnett method indicated that all tested scenarios would advance bloom's DOY. Under the reduced emission scenario (SSP1-2.6) for 2050 and 2100, the modeled bloom DOY shifted from 64 (March 5th) to 52 (February 20th) in the $\Delta T_{min \cdot max}$ model and to 51 by the ΔT_{max} scenario ($p < 0.05$). If the emissions scenarios will not change (SSP5-8.5), the $\Delta T_{min \cdot max}$model projected that bloom DOY would advance to 48 (February 17th) by 2050, and the ΔT_{max} model predicted that almond trees would bloom by DOY 49 (February 18th). Predictions for 2100 were that trees would bloom by January 28th (DOY 28) or February 2nd (DOY 33) by the $\Delta T_{min \cdot max}$and ΔT_{max} scenarios, respectively ($p < 0.0001$; Fig. 3a).

We used the new models to locate growing regions unsuitable for almond production due to future climate shifts. We considered that bloom times before February 1st (DOY 32) would jeopardize almond reproduction by frosts and limited bee activity. We also contemplated that a bloom later than March 31st (DOY 90) will reduce pollen production by high temperatures (>21°C). The models determined that over the past 40 years (1982-2022), a substantial portion (~43,500 km²) of Central Valley's total area (~47,000 km²) has been suitable for almond production. An ANOVA analysis exhibited a significant main effect of the climatic scenarios on bloom area ($F(6, 63) = 25.8$; $p < 0.0001$). Using the past as a control and conducting posthoc testing with the Dunnett method, the model suggested that there will be an insignificant reduction in the suitable land to ~37,500 km² ($p>0.6$) by 2050. However, a significant decrease in the suitable area is predicted for 2100 by the unchanged-emission scenario (SSP5-8.5), with almost all of the Central Valley becoming unfit for almond production under both $\Delta T_{min \cdot max}$ and ΔT_{max} scenarios, leaving only 6,000 km² or ~16,500 km² productive (respectively; $p<0.0001$; Figs. 3b, 4).

Discussion

The impact of climate change on tree phenology is one of the most discussed aspects of global warming [38]. Presumably, higher temperatures will result in earlier bloom. Indeed, our analysis suggests that over the last

40 years, the rate of change in the bloom of almond trees was 0.11 days year^{-1} resulting in a shift of 1.1 days over a decade. This rate of change is similar to several long-term observational studies showing that dormancy break shifted by a few days over the last few decades with a typical rate of 0.18 day year^{-1} [39–41]. Our model, which links carbohydrate content in the fall with winter temperatures to predict bloom [12,33], suggests that this trend will continue under the most optimistic CO_2 emissions scenario (SSP1-2.5) over the next few decades and stabilize by the end of the century. However, supposing no emission reduction measures are implemented (SSP5-8.5), the trend towards earlier blooms may persist or even accelerate from approximately 1.1 days per decade (observed over the past 40 years) to nearly 2.5 days per decade under the $\Delta T_{min\,|\,max}$ model conditions. This substantial shift could lead to significant losses of prime orchard areas.

In California, almond trees generally bloom between early February and late March. This period aligns with a reduced likelihood of hard frost, typically occurring from mid-December to January, which could potentially harm or destroy the flower's ovules. Furthermore, it steers clear of excessively high temperatures (above 21°C), as they present a significant barrier for almond pollen production [16]. Using these two dates as thresholds for land suitability for almond production, our analysis suggests that California's Central Valley currently provides adequate conditions for timely bloom. Moreover, it is projected that 95 percent of the area will continue to maintain favorable spring conditions for almond bloom for the next 30 years or even until the end of the century if greenhouse gas emission decrease (SSP1-2.6 scenario). However, if emissions continue to rise unchecked (SSP5 8.5), we expect a significant loss in arable lands for almond production. A 50% loss in almond production area is predicted under the ΔT_{max} scenario, and approximately 95% loss under the $\Delta T_{min|max}$ scenario. Hence, despite comforting predictions that California will be climatically favorable for almond production for the next 30 years, it appears almond farming is not immune to climate shifts. If carbon emissions are not reduced, California will not be suitable for almond production by 2100. Considering that almond orchards' longevity is 25-30 years, we might be planting the last cohort of California's almond farms.

Prior studies have indicated potential arable land losses due to insufficient water availability or changes in summer temperature [17]. Furthermore, research suggests that plant performance is more sensitive to variations in water availability or precipitation rather than extreme temperatures [18–20]. Since the majority of orchards in California's Central Valley are irrigated, any loss of farmland due to summer climate changes may not be directly attributed to temperature fluctuations, but rather to changes in water allocation or advancements in irrigation technology. Nevertheless, the impact of winter climate shifts on perennial plants is insufficiently understood by researchers or stakeholders. Changes in winter temperatures can influence the use of energy reserves (NSC) and trigger earlier blooms. These early blooms may expose plants to frost or create conditions that adversely affect pollination, thereby reducing crop potential. The loss of the most productive almond-growing area in the world, which accounts for nearly 80% of total global output, would be devastating, as similar Mediterranean-like climatic regions are scarce. Recognizing that the loss of arable lands may be inevitable, we can proactively allocate resources to develop techniques and mitigate the impact of winter temperatures on phenology. Focusing on innovative approaches and adaptive measures may preserve the productivity of these vital almond-growing regions and ensure the sustainability of almond production in the face of climate change.

Acknowledgments

We thank the US-Israel Binational Agricultural Research and Development (BARD) for funding this study, the project numb IS-5288-20.

Author Contributions

J.O & M.A.Z conceptualized project with contributions from O.S, T.P.K and O.L. J.O performed the computations, data collection, data visualization and wrote the first version of manuscript. All authors contributed to subsequent manuscript revisions.

Corresponding Author

Correspondence to Jessica Orozco

Competing interests

The authors declare no competing interests.

Data availability

Available upon request from the corresponding author, Jessica Orozco.

References

1. Yu, P. *et al.* Black carbon lofts wildfire smoke high into the stratosphere to form a persistent plume. *Science* **365**, 587–590 (2019).
2. Aguilera, R., Corringham, T., Gershunov, A. & Benmarhnia, T. Wildfire smoke impacts respiratory health more than fine particles from other sources: observational evidence from Southern California. *Nat. Commun.* **12**, 1493 (2021).
3. Roderick, M. L., Farquhar, G. D., Berry, S. L. & Noble, I. R. On the direct effect of clouds and atmospheric particles on the productivity and structure of vegetation. *Oecologia* **129**, 21–30 (2001).
4. Gilbert, M. E. & Ripley, B. S. The effect of smoke on the photosynthetic gas exchange of Chrysanthemoides monilifera. *S. Afr. J. Bot.* **68**, 525–531 (2002).
5. Mercado, L. M. *et al.* Impact of changes in diffuse radiation on the global land carbon sink. *Nature* **458**, 1014–1017 (2009).
6. Rap, A. *et al.* Fires increase Amazon forest productivity through increases in diffuse radiation. *Geophys. Res. Lett.* **42**, 4654–4662 (2015).

7. Yue, X. & Unger, N. Fire air pollution reduces global terrestrial productivity. *Nat. Commun.* **9**, 5413 (2018).

8. Yue, X. & Unger, N. Aerosol optical depth thresholds as a tool to assess diffuse radiation fertilization of the land carbon uptake in China. *Atmos. Chem. Phys.* **17**, 1329–1342 (2017).

9. Farquhar, G. D., Ehleringer, J. R. & Hubick, K. T. Carbon isotope discrimination and photosynthesis. *Annu. Rev. Plant Physiol. Plant Mol. Biol.* **40**, 503–537 (1989).

10. Felzer, B. S., Cronin, T., Reilly, J. M., Melillo, J. M. & Wang, X. Impacts of ozone on trees and crops. *C. R. Geosci.* **339**, 784–798 (2007).

11. Matthews, J. S. A., Vialet-Chabrand, S. & Lawson, T. Role of blue and red light in stomatal dynamic behaviour. *J. Exp. Bot.* **71**, 2253–2269 (2020).

12. Sperling, O. & Zwieniecki, M. A. Winding up the bloom clock—do sugar levels at senescence determine how trees respond to winter temperature? *Tree Physiol.* (2021) doi:10.1093/treephys/tpab051.

13. Zwieniecki, M. A., Davidson, A. M., Orozco, J., Cooper, K. B. & Guzman-Delgado, P. The impact of non-structural carbohydrates (NSC) concentration on yield in Prunus dulcis, Pistacia vera, and Juglans regia. *Sci. Rep.* **12**, 4360 (2022).

14. McDowell, N. G. *et al.* Mechanisms of woody-plant mortality under rising drought, CO2 and vapour pressure deficit. *Nature Reviews Earth and Environment* **3**, 294–308 (2022).

15. McDowell, N. G. Mechanisms linking drought, hydraulics, carbon metabolism, and vegetation mortality. *Plant Physiol.* **155**, 1051–1059 (2011).

16. Palácios, R. *et al.* Evaluation of MODIS Dark Target AOD Product with 3 and 10 km Resolution in Amazonia. *Atmosphere* **13**, 1742 (2022).

17. Swain, D. L. A shorter, sharper rainy season amplifies California wildfire risk. *Geophys. Res. Lett.* **48**, (2021).

18. The R Project for Statistical Computing. https://www.r-project.org/.

19. Tidy Anomaly Detection. https://business-science.github.io/anomalize/.

20. Kassambara, A. Pipe-Friendly Framework for Basic Statistical Tests [R package rstatix version 0.7.2]. (2023).
21. Lenth, R. V. Estimated Marginal Means, aka Least-Squares Means [R package emmeans version 1.8.5]. (2023).
22. CAL FIRE - California Open Data. https://data.ca.gov/dataset/cal-fire.
23. Pope, K. S. & DeJong, T. M. Modeling spring phenology and chilling requirements using the chill overlap framework. *Acta Hortic.* 179–184 (2017).
24. Friedl, M. A. *et al.* A tale of two springs: using recent climate anomalies to characterize the sensitivity of temperate forest phenology to climate change. *Environ. Res. Lett.* **9**, 054006 (2014).
25. Taylor, S. D., Meiners, J. M., Riemer, K., Orr, M. C. & White, E. P. Comparison of large-scale citizen science data and long-term study data for phenology modeling. *Ecology* **100**, e02568 (2019).
26. Aono, Y. & Saito, S. Clarifying springtime temperature reconstructions of the medieval period by gap-filling the cherry blossom phenological data series at Kyoto, Japan. *Int. J. Biometeorol.* **54**, 211–219 (2010).
27. Aono, Y. & Kazui, K. Phenological data series of cherry tree flowering in Kyoto, Japan, and its application to reconstruction of springtime temperatures since the 9th century. *Int. J. Climatol.* **28**, 905–914 (2008).
28. Richardson, A. D., Bailey, A. S., Denny, E. G., Martin, C. W. & O'keefe, J. Phenology of a northern hardwood forest canopy. *Glob. Chang. Biol.* **12**, 1174–1188 (2006).
29. Zohner, C. M., Mo, L. & Renner, S. S. Global warming reduces leaf-out and flowering synchrony among individuals. *Elife* **7**, (2018).
30. Luedeling, E., Zhang, M. & Girvetz, E. H. Climatic changes lead to declining winter chill for fruit and nut trees in California during 1950-2099. *PLoS One* **4**, e6166 (2009).
31. Luedeling, E., Guo, L., Dai, J., Leslie, C. & Blanke, M. M. Differential responses of trees to temperature variation during the chilling and forcing phases. *Agric. For. Meteorol.* **181**, 33–42 (2013).

32. Luedeling, E., Kunz, A. & Blanke, M. M. Identification of chilling and heat requirements of cherry trees—a statistical approach. *Int. J. Biometeorol.* **57**, 679–689 (2013).

33. Sperling, O. *et al.* Predicting bloom dates by temperature mediated kinetics of carbohydrate metabolism in deciduous trees. *Agric. For. Meteorol.* **276–277**, 107643 (2019).

34. Nazarenko, L. S. *et al.* Future Climate Change Under SSP Emission Scenarios With GISS-E2.1. *Journal of Advances in Modeling Earth Systems* **14**, e2021MS002871 (2022).

35. Woldearegay, M. & Department of Biology, Debre Birhan University, P. O. Box 445, Debre Birhan, Ethiopia. Climate change impacts on the distribution and phenology of plants: A review. *Trop. Plant Res.* **7**, 196–204 (2020).

36. Inouye, D. W. Climate change and phenology. *Wiley Interdiscip. Rev. Clim. Change* **13**, (2022).

37. Vezvaei, A. Pollen tube growth in Nonpareil almond in relation to pollen genotype, temperature and competition among mixed pollen. in *II International Symposium on Pistachios and Almonds 470* 251–261 (actahort.org, 1997).

38. Pathak, T. B. *et al.* Climate Change Trends and Impacts on California Agriculture: A Detailed Review. *Agronomy* **8**, 25 (2018).

39. Yin, J. *et al.* Future socio-ecosystem productivity threatened by compound drought–heatwave events. *Nature Sustainability* **6**, 259–272 (2023).

40. Troy, T. J., Kipgen, C. & Pal, I. The impact of climate extremes and irrigation on US crop yields. *Environ. Res. Lett.* **10**, 054013 (2015).

41. Zanotelli, D., Montagnani, L., Andreotti, C. & Tagliavini, M. Water and carbon fluxes in an apple orchard during heat waves. *Eur. J. Agron.* **134**, 126460 (2022).

Figure 1: Historic winter climate conditions. a) Average daily maximum temperature (t_max) and average daily minimum temperature (t_min) in Central Valley, CA, USA, between 1982 and 2022 from October 15 to April 30. There was a significant upward trend of t_max but not in t_min. **b**) Change in the standard deviations of t_max and t_min in Central Valley, CA, USA, between 1982 and 2022. There was a significant upward trend of t_min std but not in t_min.

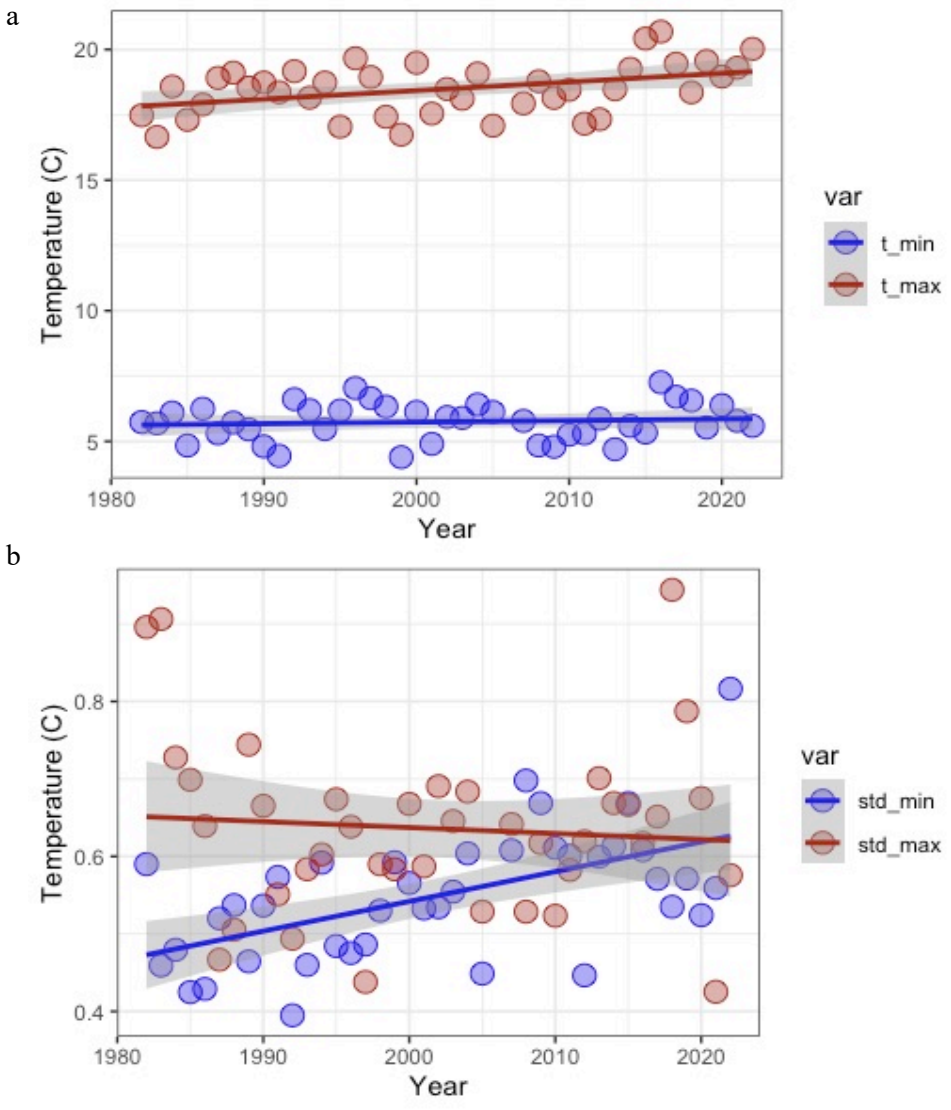

Figure 2: Historic bloom time projections. a) Modeled average historic bloom day of the year (DOY) for Central Valley, CA. **b**) Density plot of bloom DOY across California's almond growing regions. **c**) Four examples of bloom DOY across Central Valley, CA, depicting synchronous (1985 and 2004) and asynchronous (1982 and 1999) bloom patterns.

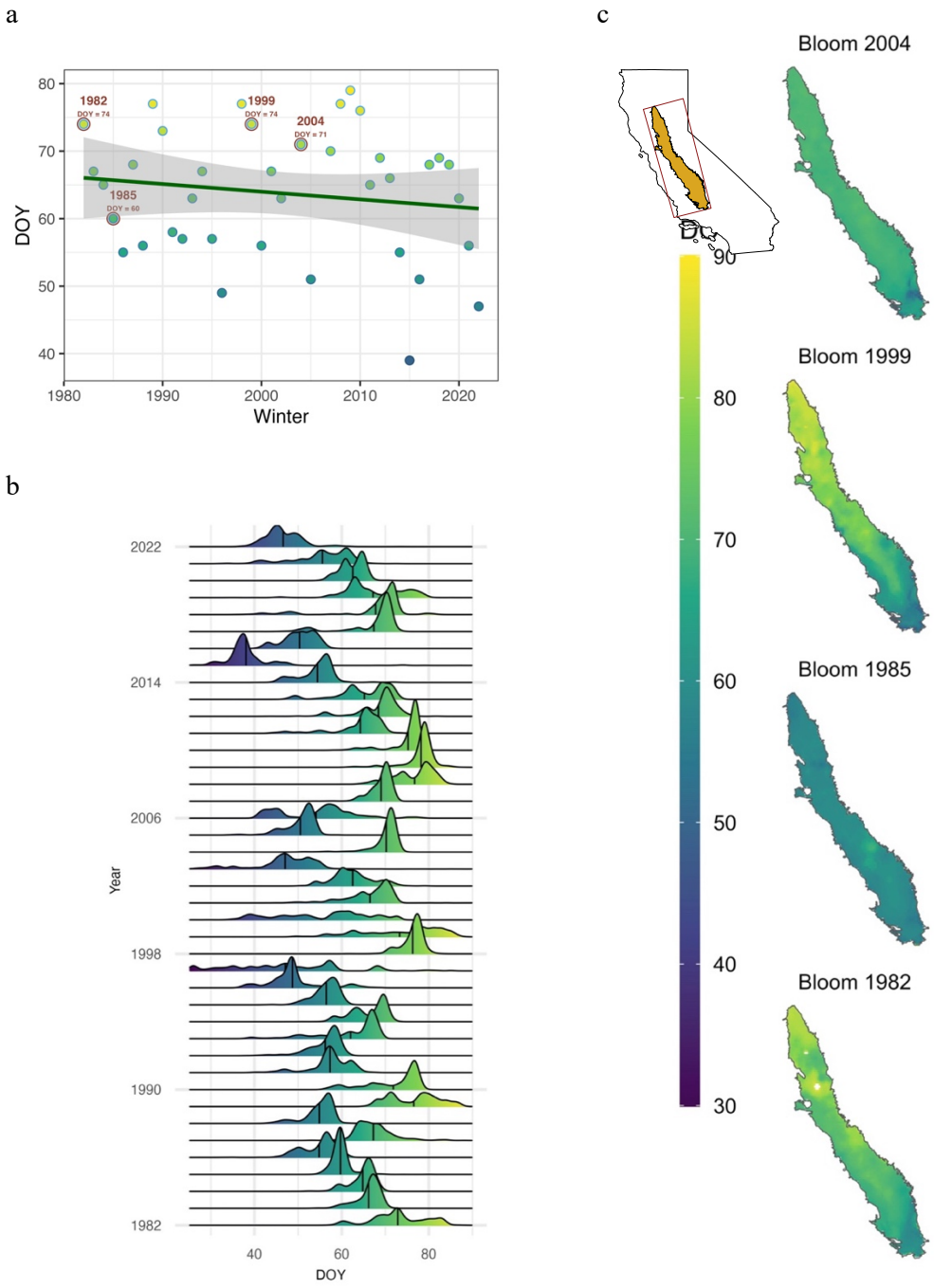

.

Figure 3: Predictions of future almond bloom time under different scenerios. a) Modeled average bloom day of year (DOY) for each scenario and **b**) The total area supporting bloom in Central Valley, CA, spans from February 1st (DOY 32) to March 31st (DOY 90) given the respective model.

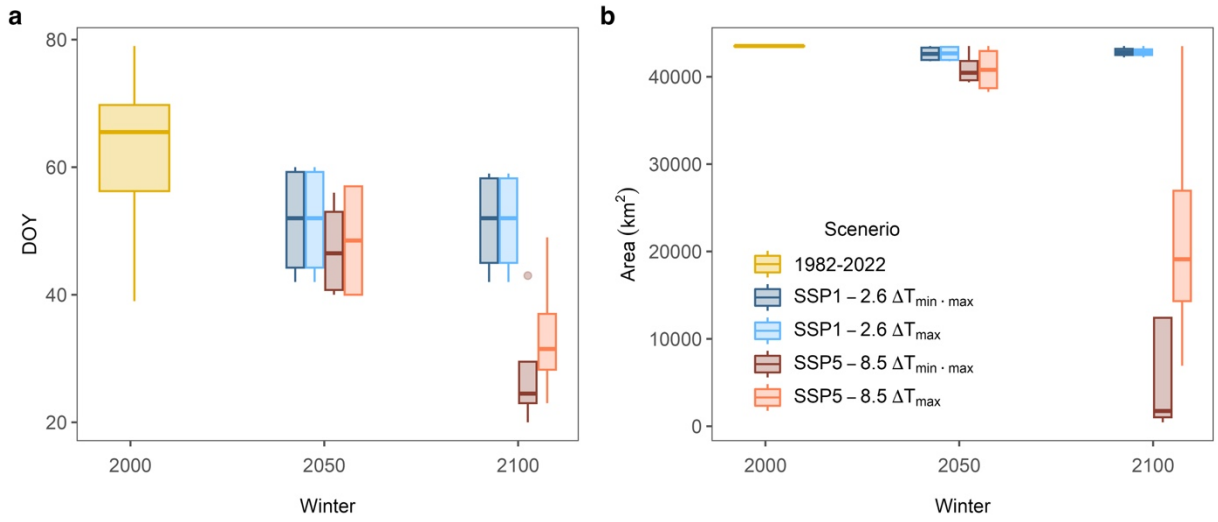

Figure 4: Projected spatial variability in almond bloom time. Bloom day of the year (DOY) between 32 (February 1st) and 90 (April 1st) across the California Central Valley. The first row demonstrates projected historical bloom data. The following two rows depict bloom predictions for 2050 and 2100 respectively. To account for year-to-year variability, we conducted four different simulations for 2050 and 2100 based on the winters of 2019, 2020, 2021 and 2022. The white area represents land area unsuitable for almond production.

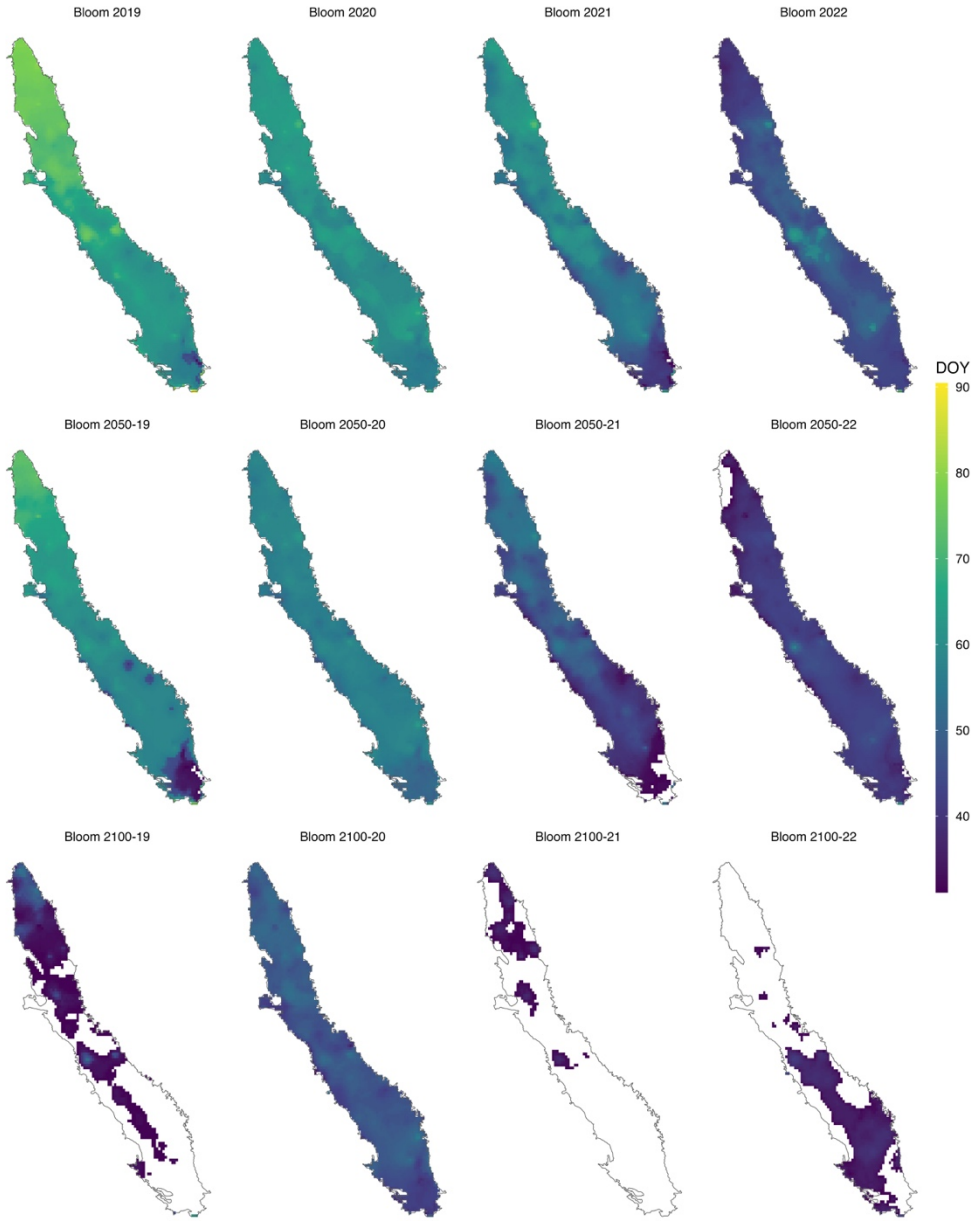

Conclusions

Here, I present three unique research endeavors that utilize non-structural carbohydrate (NSC) measurements as a tool to evaluate plant responses to varying environmental conditions.

In the first chapter, the focus of our research was to discern how the rate of stress development influences energy reserves and impacts the recovery process. In this context, we exposed Grenache, a *Vitis vinifera* cultivar, to two different drought development rates - a fast-developing drought (FDD, typical of controlled pot experiments, and a slow-developing drought (SDD), which is more typical of natural conditions. FDD, characterized by rapid stomatal closure (2-3 days) in response to escalated stress levels and high abscisic acid (ABA) accumulation in xylem sap, didn't show substantial changes associated with stem priming for recovery. SDD, on the other hand, was marked by a gradual stomatal closure, low ABA accumulation, and changes that prepared the stem for recovery, including xylem sap acidification and sugar accumulation. While both FDD and SDD exhibited similar trends over time concerning the recovery of stomatal conductance, they varied in their sensitivity to xylem ABA. Interestingly, Grenache showcased near-isohydric behavior during fast-developing droughts, potentially offering protection against abrupt tension fluctuations. However, the plant transitioned to a near-anisohydric behavior during slow-developing droughts, prioritizing the preservation of photosynthetic activity over hydraulic safety.

The impact of drought treatments on the total non-structural carbohydrate (NSC) content in plant stems varied. The fast-developing drought (FDD) treatment didn't alter the total carbohydrate content (starch plus soluble sugars) in stem tissues throughout the stress and recovery period. However, plants exposed to slow-developing drought (SDD) witnessed an increase in total

NSC content during stress, which subsequently returned to pre-stress levels upon water alleviation. Here, the sugar concentration resembled that of well-watered grapevines.

Looking closely, FDD treatment resulted in a noticeable increase in stem starch content during the drought imposition (1.5-fold more than controls) and after a day of re-watering (2.2-fold more). There was, however, no significant change in soluble sugar accumulation throughout the experiment. Plants under SDD treatment accumulated slightly more starch compared to well-watered conditions and significantly more soluble sugars (1.7-fold more). Notably, stem sugar levels in SDD plants returned to pre-stress levels within a day of recovery, illustrating the adaptability of plants to stress conditions and their subsequent resilience upon recovery.

This differential response based on the progression rate of drought underscores that plants enduring long-term drought are capable of adapting uniquely. These results accentuate the importance of employing a stress application pattern that accurately reflects field conditions when conducting studies on plant responses to drought.

In the second chapter of our research, we present a pioneering analysis investigating the effects of prolonged smoke exposure on plant health under natural field conditions. Our primary focus was to understand the relationship between extended smoke exposure and the non-structural carbohydrate (NSC) reserves in trees. Utilizing a comprehensive regional dataset combined with detailed spatiotemporal satellite data, we highlight the detrimental impact of dense smoke plumes on vegetation.

Our findings demonstrate that when smoke exposure takes place during the mid-growth (August) season, it may lead to a transient decline in the plants' non-structural carbohydrate reserves. On the other hand, if plants encounter such exposure later in their growth cycle, specifically in September, it can disrupt the vital process of carbohydrate reserve buildup that precedes their

dormant stage. This could manifest as a prolonged reduction in carbohydrate reserves, particularly if smoke coincides with the period when plants are bolstering their reserves for dormancy, thereby leaving lasting impacts. This insight unveils a previously unrecognized risk to plant health and ecosystem stability across various landscapes, raising significant concerns. Extended smoke exposure could cause potential damage to both agricultural and natural environments on a regional scale, highlighting the importance of understanding and mitigating such risks.

Finally, in the final chapter, we explore the potential implications of climate change on almond orchards' phenology and the subsequent suitability of land for almond farming. We utilize historical climate data, a comprehensive model incorporating daily minimum/maximum temperatures and non-structural carbohydrate dynamics in twigs, and CMIP6 climate predictions to anticipate variations in bloom times within California's Central Valley. We conducted our analysis under two distinct climate change scenarios: the first one, SSP1-2.6, presupposes a gradual reduction in emissions, leading to a limited warming of 1.4°C, while the second, SSP5-8.5, assumes a static emission pathway with an average warming of 5°C.

Our findings project that the land suitable for almond farming will remain largely stable over the next three decades. However, under the unchanged emission scenario (SSP5-8.5), the suitable land for almond farming could witness a stark reduction ranging from 50% to 95% by the century's end. This drop aligns with a projected shift in bloom time, transitioning from the historically observed average 64th Day of the Year (DOY), to a notably earlier period, between DOY 28-33 by 2100. These predictions underscore the crucial role climate change plays in shaping almond production's future in the Central Valley, California. It emphasizes the pressing need to understand and address these changes for sustainable agricultural land management, ensuring long-term food security and economic stability amidst a rapidly evolving climate scenario.